

Variational Autoencoders for Efficient Simulation-Based Inference

Mayank Nautiyal¹, Andrey Shternshis¹, Andreas Hellander², and Prashant Singh¹

¹Science for Life Laboratory, Uppsala University

²Uppsala University

Abstract

We present a generative modeling approach based on the variational inference framework for likelihood-free simulation-based inference. The method leverages latent variables within variational autoencoders to efficiently estimate complex posterior distributions arising from stochastic simulations. We explore two variations of this approach distinguished by their treatment of the prior distribution. The first model adapts the prior based on observed data using a multivariate prior network, enhancing generalization across various posterior queries. In contrast, the second model utilizes a standard Gaussian prior, offering simplicity while still effectively capturing complex posterior distributions. We demonstrate the efficacy of these models on well-established benchmark problems, achieving results comparable to flow-based approaches while maintaining computational efficiency and scalability.

1 Introduction

The simulation-based inference (SBI) problem involves statistical inference of parameters θ of a stochastic simulation model $M(\theta, \xi)$ containing random states ξ , from observed data \mathbf{y} [Cranmer et al., 2020]. Once calibrated, the simulation model can be used to reason about, analyze and explain the observed data \mathbf{y} in the context of the corresponding physical process [Lavin et al., 2021]. Several challenges arise in SBI owing to model stochasticity and potential multi-valuedness, where different sets of parameter values can produce similar observations, or similar parameters may lead to varied outputs. Consequently, the task is to infer the posterior distribution $p(\theta | \mathbf{y})$ in a Bayesian setting.

A user-defined prior distribution $p(\theta)$ encodes domain knowledge or assumptions about plausible parameter values. The likelihood function $p(\mathbf{y} | \theta)$ is however, often intractable due to intricate stochastic dynamics, high-dimensional integration, or latent variables making analytical computation impractical [Sisson et al., 2018]. Although a closed-form expression for the likelihood function $p(\mathbf{y} | \theta)$ is unavailable, samples

from this distribution can be generated by evaluating the simulator M with varying ξ for different θ drawn from the prior, effectively yielding samples from the joint distribution $(\theta, \mathbf{y}) \sim p(\theta, \mathbf{y})$.

Deep learning based approaches that directly approximate the model likelihood, or the posterior distribution have gained increasing popularity in the SBI setting [Zammit-Mangion et al., 2024]. Several approaches involve flow-based models, which are potentially compute-intensive and also restrict the design space of neural networks to invertible functions with computationally efficient Jacobian calculations [Rezende and Mohamed, 2015]. This constraint can limit the flexibility of the model in handling more complex data structures. Alternative approaches like Generative Adversarial Training for SBI (GATSBI) [Ramesh et al., 2022] use an adversarial network, where a generator produces simulations that mimic observed data, and a discriminator distinguishes between real and simulated data. However, the adversarial approach can suffer from training instability, mode collapse, and difficulties in balancing the generator and discriminator networks [Arjovsky and Bottou, 2022, Arjovsky et al., 2017], complicating training and limiting robustness.

Contribution: We propose a variational inference approach for simulation-based inference, utilizing a Conditional Variational Autoencoder (C-VAE) architecture [Kingma and Welling, 2014, Sohn et al., 2015] that is simple, computational efficient, scalable, interpretable and robust. As VAEs are not constrained by the invertibility requirement, they allow seamless integration of various neural network architectures without significant modifications as opposed to flow-based models. VAEs also avoid the instability associated with GANs due to adversarial learning dynamics. As a result, C-VAEs can handle complex data structures and dependencies more effectively, making them suitable for a wider range of tasks without requiring external summary networks [Cranmer et al., 2020].

The paper is organized as follows. Section 2 outlines the related work. In Section 3, we provide a formal problem definition, followed by a detailed explanation

of the proposed architecture in Sections 3.1 and 3.2. A comprehensive comparison on benchmark test problems is presented in Section 4 and in the Appendix. Section 5 discusses the results, while Section 6 concludes the paper by summarizing the key findings and further advancements.

2 Related Work

A vast majority of SBI approaches based on deep learning aim to either approximate the likelihood [Hermans et al., 2020], or focus on directly approximating the posterior [Papamakarios and Murray, 2016, Lueckmann et al., 2017, Greenberg et al., 2019]. Additionally, there exist methods that target both the likelihood and posterior simultaneously [Radev et al., 2023a, Glöckler et al., 2022, Wqvist et al., 2021]

Neural Posterior Estimation (NPE) [Papamakarios and Murray, 2016] was one of the earliest approaches towards one-step posterior estimation, introducing the use of conditional normalizing flows to approximate the posterior distribution. By incorporating techniques such as Neural Spline Flows (NSFs) and Mixture Density Networks (MDNs), NPE enhanced both the accuracy and scalability of simulation-based inference. In comparison to traditional approaches like Approximate Bayesian Computation (ABC) or Sequential Monte-Carlo (SMC)-ABC [Sisson et al., 2018] that rely on repeated simulations and rejection-based schemes, NPE and its derivatives such as Robust NPE [Ward et al., 2022] are more efficient and flexible.

Sequential Neural Posterior Estimation (SNPE) improves NPE’s efficiency by employing sequential training, where initial parameters are sampled from the prior, and the model is iteratively refined by focusing on regions of the parameter space that are most relevant to the parameter inference task. This adaptive sampling allows for more efficient exploration of the posterior distribution. Early versions like SNPE-A [Papamakarios and Murray, 2016] and SNPE-B [Lueckmann et al., 2017] required correction steps to account for changes in the sampling distribution, adding complexity to the process. In contrast, Automatic Posterior Transformation (APT) or SNPE-C [Greenberg et al., 2019], eliminated this need, offering a more robust and streamlined approach by leveraging normalizing flows to refine the posterior iteratively. However, a limitation of sequential methods like APT is that they necessitate multiple rounds of training, extending the total training time.

The recently proposed Jointly Amortized Neural Approximation (JANA) framework [Radev et al., 2023a] addresses posterior and likelihood estimation through joint amortization. JANA employs conditional invertible neural networks (cINNs) for both the

posterior and likelihood networks, allowing efficient transformations between the parameter space and latent variables. Additionally, JANA includes a trainable summary network sub-module optimized to extract maximally informative data representations in an end-to-end manner. Unlike previous approaches, JANA follows a fully amortized strategy, allowing the evaluation of normalized densities and generation of conditional random draws for parameter estimation and surrogate modeling. Simformer [Glöckler et al.] is a recent approach that leverages a probabilistic diffusion model with transformer architectures to accurately learn complex, high-dimensional posteriors, making it highly flexible. However, the transformer-based architecture is relatively resource-intensive and involves careful optimization.

We compare our proposed approach with four popular SBI methods: JANA [Radev et al., 2023a], GATSBI [Ramesh et al., 2022], APT [Greenberg et al., 2019], and NPE [Papamakarios and Murray, 2016]. The motivation is to cover a variety of approaches (e.g., flow-based, adversarial, one-shot, sequential) while noting that our focus is on efficiency and scalability as opposed to solely the posterior approximation accuracy. We refer the reader to [Zammit-Mangion et al., 2024] and [Radev et al., 2023a] for further reading on deep learning methods for SBI.

3 Simulation Based Inference

In the Bayesian framework, the aim is to infer the posterior distribution $p(\boldsymbol{\theta} \mid \mathbf{y})$ over the model parameters $\boldsymbol{\theta}$, given the observed data \mathbf{y} . From Bayes’ theorem, the posterior distribution can be expressed as:

$$p(\boldsymbol{\theta} \mid \mathbf{y}) = \frac{p(\mathbf{y} \mid \boldsymbol{\theta})p(\boldsymbol{\theta})}{p(\mathbf{y})}, \quad (1)$$

where $p(\mathbf{y}) = \int p(\mathbf{y} \mid \boldsymbol{\theta})p(\boldsymbol{\theta}) d\boldsymbol{\theta}$ is the marginal likelihood, acting as a normalizing constant to ensure that the posterior is a valid probability distribution. However, as $p(\mathbf{y})$ does not depend upon $\boldsymbol{\theta}$, it can be ignored in the computations involving the posterior.

We propose two models for amortized inference: a Conditional Prior VAE (CP-VAE) and an Unconditional Prior VAE (UP-VAE). Both models utilize latent variables to capture hidden structures in the data. The Conditional Prior VAE uses a multivariate prior network that conditions on observed data, enabling adaptive inference that improves generalization across posterior queries. The Unconditional Prior VAE, in contrast, employs a simpler Gaussian prior with unit variance, while still capturing complex posterior distributions. Leveraging the variational inference framework, both models achieve competitive performance

across a range of tasks, including bimodal and high-dimensional settings.

3.1 Conditional Prior VAE (CP-VAE)

The Conditional Prior Variational Autoencoder (CP-VAE) is an extension of the standard Conditional Variational Autoencoder (CVAE) [Sohn et al., 2015, Ivanov et al., 2019] specifically designed for simulation-based inference. We begin by introducing an auxiliary latent variable \mathbf{z} to capture complex structures and dependencies within the joint distribution $p(\boldsymbol{\theta}, \mathbf{y})$ of parameters $\boldsymbol{\theta}$ and simulated data \mathbf{y} . The latent variable \mathbf{z} serves as a learned, low-dimensional summary statistic, efficiently encoding the most salient features of high-dimensional data relevant to characterize the posterior distribution. We formulate a latent variable model $p(\mathbf{z} | \mathbf{y}, \boldsymbol{\theta})$ and approximate it using a variational distribution $q_\psi(\mathbf{z} | \mathbf{y}, \boldsymbol{\theta})$, parameterized by $\psi \in \Phi$, where Φ represents a family of distributions. The goal is to minimize the Kullback-Leibler (KL) divergence between this variational distribution and the true conditional distribution [Jordan et al., 1999, Kingma and Welling, 2014]:

$$\min_{\psi \in \Phi} D_{KL} \left(q_\psi(\mathbf{z} | \mathbf{y}, \boldsymbol{\theta}) \| p(\mathbf{z} | \mathbf{y}, \boldsymbol{\theta}) \right). \quad (2)$$

Using Bayes' theorem and the chain rule of probability, the conditional distribution $p(\mathbf{z} | \mathbf{y}, \boldsymbol{\theta})$ becomes:

$$p(\mathbf{z} | \mathbf{y}, \boldsymbol{\theta}) = \frac{p(\boldsymbol{\theta} | \mathbf{z}, \mathbf{y}) p(\mathbf{z} | \mathbf{y})}{p(\boldsymbol{\theta} | \mathbf{y})}. \quad (3)$$

Substituting (3) into (2), and denoting the KL divergence $D_{KL}(q_\psi(\mathbf{z} | \mathbf{y}, \boldsymbol{\theta}) \| p(\mathbf{z} | \mathbf{y}, \boldsymbol{\theta}))$ as \mathcal{D} , we obtain:

$$\mathcal{D} = \mathbb{E}_{\mathbf{z} \sim q_\psi(\mathbf{z} | \mathbf{y}, \boldsymbol{\theta})} \left[\log q_\psi(\mathbf{z} | \mathbf{y}, \boldsymbol{\theta}) - \log p(\mathbf{z} | \mathbf{y}) - \log p(\boldsymbol{\theta} | \mathbf{y}, \mathbf{z}) + \log p(\boldsymbol{\theta} | \mathbf{y}) \right]. \quad (4)$$

Rearranging the components of equation (4), we isolate $\log p(\boldsymbol{\theta} | \mathbf{y})$ to derive:

$$\log p(\boldsymbol{\theta} | \mathbf{y}) \geq -D_{KL} \left(q_\psi(\mathbf{z} | \mathbf{y}, \boldsymbol{\theta}) \| p(\mathbf{z} | \mathbf{y}) \right) + \mathbb{E}_{\mathbf{z} \sim q_\psi(\mathbf{z} | \mathbf{y}, \boldsymbol{\theta})} \left[\log p(\boldsymbol{\theta} | \mathbf{y}, \mathbf{z}) \right]. \quad (5)$$

This inequality stems from the fundamental non-negativity property of the KL divergence, establishing a lower bound on the log-posterior $p(\boldsymbol{\theta} | \mathbf{y})$. This bound forms the core of the optimization objective in the CP-VAE framework. Maximizing the log-posterior can be conveniently reformulated as minimizing its

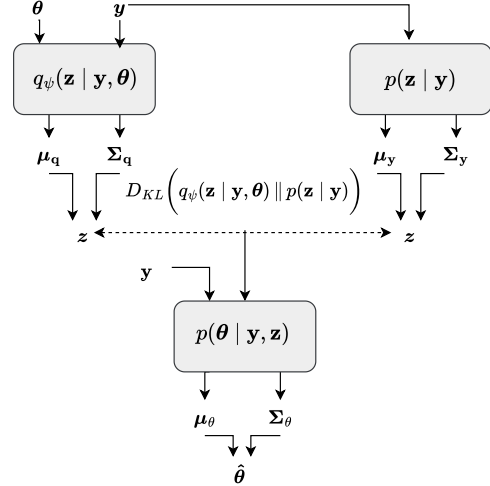


Figure 1: CP-VAE Architecture. The encoder $q_\psi(\mathbf{z} | \mathbf{y}, \boldsymbol{\theta})$ computes the parameters of the variational distribution for latent variables \mathbf{z} , conditioned on paired simulated data \mathbf{y} and parameters $\boldsymbol{\theta}$. The prior network $p(\mathbf{z} | \mathbf{y})$ defines a data-dependent prior over \mathbf{z} , enforcing latent space regularization via the KL divergence. The decoder $p(\boldsymbol{\theta} | \mathbf{y}, \mathbf{z})$ generates the distribution parameters for $\boldsymbol{\theta}$ based on \mathbf{y} and \mathbf{z} . Both \mathbf{z} and $\boldsymbol{\theta}$ are sampled using the reparameterization trick, ensuring end-to-end differentiability.

negative, which is a standard approach in optimization, leading to the following formulation:

$$\mathcal{L}(\boldsymbol{\theta}, \mathbf{y}; \psi) = D_{KL} \left(q_\psi(\mathbf{z} | \mathbf{y}, \boldsymbol{\theta}) \| p(\mathbf{z} | \mathbf{y}) \right) - \mathbb{E}_{\mathbf{z} \sim q_\psi(\mathbf{z} | \mathbf{y}, \boldsymbol{\theta})} \left[\log p(\boldsymbol{\theta} | \mathbf{y}, \mathbf{z}) \right]. \quad (6)$$

The key advantage of this formulation lies in the prior distribution $p(\mathbf{z} | \mathbf{y})$ being conditioned on the observed data \mathbf{y} , allowing the model to adaptively shape its latent representation based on observed data, a crucial feature for effective amortized inference. This adaptive prior serves as a powerful regularization mechanism, ensuring that the latent space accurately captures the relevant features from the joint distribution $p(\boldsymbol{\theta}, \mathbf{y})$. As a result, this approach delivers more precise posterior approximations, especially when dealing with data that exhibit complex conditional dependencies, which a fixed prior cannot adequately capture. Such adaptability is crucial for models aiming to generalize across a wide range of queries, making the CP-VAE framework well-suited for real-world applications with intricate data dependencies [Sohn et al., 2015].

The loss function presented in (6) is generally intractable due to the complexity of computing both the KL divergence between the variational distribu-

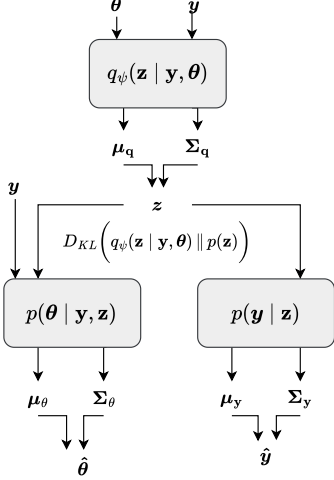


Figure 2: UP-VAE architecture. The encoder $q_\psi(\mathbf{z} | \mathbf{y}, \boldsymbol{\theta})$ outputs the mean and variance of the approximate distribution, from which \mathbf{z} is sampled (reparameterization trick). The KL divergence is computed between the encoder output and a standard normal prior. The theta decoder $p(\boldsymbol{\theta} | \mathbf{y}, \mathbf{z})$ outputs the parameters for $\boldsymbol{\theta}$, and the data decoder $p(\mathbf{y} | \mathbf{z})$ outputs the parameters for \mathbf{y} (reparameterization trick).

tion $q_\psi(\mathbf{z} | \mathbf{y}, \boldsymbol{\theta})$ and the true conditional prior $p(\mathbf{z} | \mathbf{y})$, as well as the expectation over the latent variable \mathbf{z} . To make the optimization process tractable, we approximate the prior distribution $p(\mathbf{z} | \mathbf{y})$, the encoder distribution $q_\psi(\mathbf{z} | \mathbf{y}, \boldsymbol{\theta})$, and the decoder distribution $p(\boldsymbol{\theta} | \mathbf{y}, \mathbf{z})$ using multivariate Gaussian distributions, each characterized by a mean vector and a covariance matrix. Since each dimension is assumed to be independent, we use a diagonal covariance matrix, which simplifies the calculation of KL divergence. The architecture of the model is illustrated in Figure 1. Detailed derivation of the loss function, along with further explanations of the underlying assumptions, are provided in Section 1 of the Appendix.

To perform amortized inference with CP-VAE for a new observation \mathbf{y}_0 , we first sample N latent variables $\{\mathbf{z}^{(i)}\}_{i=1}^N$ from the conditional prior $p(\mathbf{z} | \mathbf{y}_0)$ using the reparameterization trick [Kingma and Welling, 2014]. For each latent variable $\mathbf{z}^{(i)}$, the decoder generates the mean and variance of the parameters, from which $\boldsymbol{\theta}^{(i)}$ is then sampled via reparameterization. By aggregating a large number of such samples, we can empirically approximate $p(\boldsymbol{\theta} | \mathbf{y}_0)$, enabling statistical analysis and inference of $\boldsymbol{\theta}$ based on the observed data. The conditional prior, which is dependent on \mathbf{y}_0 , allows the model to adapt its latent representation to the specific data, while the generative decoder maps latent variables to the parameter space, enabling CP-VAE to model complex, data-dependent relationships.

3.2 Unconditional Prior VAE (UP-VAE)

A simpler alternative optimization scheme is also proposed, that employs an unconditional prior, in contrast to the earlier approach where the prior was conditioned on the observed data \mathbf{y} . Conditioning the prior on \mathbf{y} is beneficial for amortized inference, but adds additional complexity to the model as the prior now depends on the data, potentially increasing the computational burden and complicating inference. Moreover, a data-dependent prior can become overly tailored to the training data, reducing the model’s ability to generalize to new observations. By utilizing an unconditional prior, we simplify the model architecture and promote better generalization by preventing overfitting to training data. To address this, we use Bayes’ theorem to reformulate the conditional distribution $p(\mathbf{z} | \boldsymbol{\theta}, \mathbf{y})$ as:

$$p(\mathbf{z} | \boldsymbol{\theta}, \mathbf{y}) = \frac{p(\boldsymbol{\theta}, \mathbf{y} | \mathbf{z})p(\mathbf{z})}{p(\boldsymbol{\theta}, \mathbf{y})}. \quad (7)$$

Substituting (7) into the KL divergence formulation in (2), and denoting $D_{KL}(q_\psi(\mathbf{z} | \mathbf{y}, \boldsymbol{\theta}) || p(\mathbf{z} | \mathbf{y}, \boldsymbol{\theta}))$ as \mathcal{D} ,

$$\begin{aligned} \mathcal{D} = & \mathbb{E}_{\mathbf{z} \sim q_\psi} \left[\log q_\psi(\mathbf{z} | \boldsymbol{\theta}, \mathbf{y}) - \log p(\mathbf{z}) \right] \\ & - \mathbb{E}_{\mathbf{z} \sim q_\psi} \left[\log p(\boldsymbol{\theta}, \mathbf{y} | \mathbf{z}) - \log p(\boldsymbol{\theta}, \mathbf{y}) \right]. \end{aligned} \quad (8)$$

Applying the chain rule to the joint probability $p(\boldsymbol{\theta}, \mathbf{y}) = p(\mathbf{y})p(\boldsymbol{\theta} | \mathbf{y})$ and recognizing that $\log p(\mathbf{y})$ is a constant with respect to $\boldsymbol{\theta}$, along with the non-negativity property of the KL divergence, we obtain:

$$\begin{aligned} \log p(\boldsymbol{\theta} | \mathbf{y}) \geq & \mathbb{E}_{\mathbf{z} \sim q_\psi} \left[\log p(\boldsymbol{\theta} | \mathbf{y}, \mathbf{z}) + \log p(\mathbf{y} | \mathbf{z}) \right] \\ & - D_{KL} \left(q_\psi(\mathbf{z} | \boldsymbol{\theta}, \mathbf{y}) || p(\mathbf{z}) \right). \end{aligned} \quad (9)$$

Similar to (5), minimizing the negative of the right-hand side of the derived inequality is equivalent to minimizing the negative log-posterior. This aligns with our primary objective and thus, the final optimization problem can be expressed as:

$$\begin{aligned} \mathcal{L}(\boldsymbol{\theta}, \mathbf{y}; \psi) = & D_{KL}(q_\psi(\mathbf{z} | \boldsymbol{\theta}, \mathbf{y}) || p(\mathbf{z})) \\ & - \mathbb{E}_{\mathbf{z} \sim q_\psi} \left[\log p(\boldsymbol{\theta} | \mathbf{y}, \mathbf{z}) \right] \\ & - \mathbb{E}_{\mathbf{z} \sim q_\psi} \left[\log p(\mathbf{y} | \mathbf{z}) \right]. \end{aligned} \quad (10)$$

This formulation employs two decoder networks: one for reconstructing the parameters $\boldsymbol{\theta}$, and another for reconstructing the observed data \mathbf{y} . The data decoder introduces an auxiliary loss, which complements the primary loss from the parameter decoder. This auxiliary objective helps the model capture latent space

features that are informative for both θ and \mathbf{y} [Sheth and Kahou, 2024]. However, for amortized inference, only the parameter decoder is needed, as it directly generates the parameter estimates conditioned on the observed data. Similar to CP-VAE, we approximate the prior $p(\mathbf{z})$, the encoder $q_\psi(\mathbf{z} | \theta, \mathbf{y})$, the parameter decoder $p(\theta | \mathbf{y}, \mathbf{z})$, and the data decoder $p(\mathbf{y} | \mathbf{z})$ using Gaussian distributions, simplifying the computation of intractable terms. The architecture of the model is depicted in Figure 2. The derivation of the loss function and the model’s distributional assumptions are provided in Section 2 of the Appendix.

Amortized inference using UP-VAE proceeds by first sampling N latent variables $\{\mathbf{z}^{(i)}\}_{i=1}^N$ from the unconditional prior $p(\mathbf{z})$. These latent variables, along with the observed data \mathbf{y}_0 , are then input into the trained theta decoder $p(\theta | \mathbf{y}_0, \mathbf{z}^{(i)})$, which outputs the parameters of the theta distribution from which $\theta^{(i)}$ are sampled. Aggregating these samples empirically approximates $p(\theta | \mathbf{y}_0)$ in an efficient manner.

4 Experiments

We evaluate the proposed approach on ten benchmark problems from the `sbibm` suite [Lueckmann et al., 2021], each presenting unique challenges for simulation-based inference. The main text focuses on three test problems described in the following subsections. A deeper description of the problems, and additional results for the remaining benchmarks are presented in the Appendix.

For each test problem, the simulation budgets is varied in $\{10,000, 20,000, 30,000\}$. We then estimate the posterior distributions by generating 10,000 samples from fixed observed data across five independent runs. To evaluate the accuracy of the posterior approximations, we compare them against reference posteriors obtained via MCMC sampling, using the Maximum Mean Discrepancy (MMD) and the Classifier Two-Sample Test (C2ST) [Friedman, 2003] as evaluation metrics. For consistency and reproducibility, we utilized pre-generated observed data and reference posteriors from the `sbibm` library [Lueckmann et al., 2021]. Detailed hyperparameter settings for each method are provided in the Appendix. The C2ST metric computations follow Lueckmann et al. [2021] – a C2ST score close to 0.5 indicates that the two distributions are indistinguishable, whereas a score significantly higher than 0.5 suggests notable differences. The MMD calculation were performed using the BayesFlow framework [Radev et al., 2023b]. All experiments were performed on a machine with 2×16 core Intel(R) Xeon(R) Gold 6226R CPU, 576GB RAM and a NVIDIA Tesla T4 GPU (16 GB RAM).

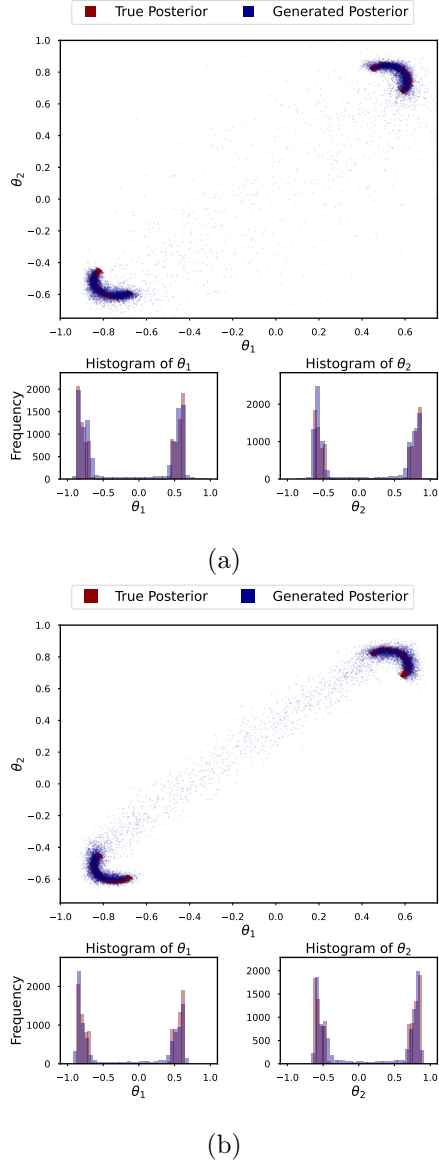


Figure 3: Two moons: true v/s estimated posterior (sim. budget: 10,000). (a) CP-VAE and (b) UP-VAE

4.1 The Two Moons Model

The Two Moons model is a popular benchmark commonly used to evaluate the ability of SBI algorithms to recover multimodal and unconventional posterior distributions [Greenberg et al., 2019, Lueckmann et al., 2021]. The challenge herein is to recover the bimodal nature of the posterior, and to capture its distinctive crescent shape. The parameter vector $\theta \sim \mathcal{U}(-1, 1)^2$ governs the model, and the observed data \mathbf{x} is generated as:

$$\mathbf{x} | \theta = \begin{pmatrix} r \cos(a) + 0.25 \\ r \sin(a) \end{pmatrix} + \frac{1}{\sqrt{2}} \begin{pmatrix} -|\theta_1 + \theta_2| \\ -(\theta_1 - \theta_2) \end{pmatrix}, \quad (11)$$

for radius $r \sim \mathcal{N}(0.1, 0.01^2)$ and angle $a \sim \mathcal{U}(-\frac{\pi}{2}, \frac{\pi}{2})$.

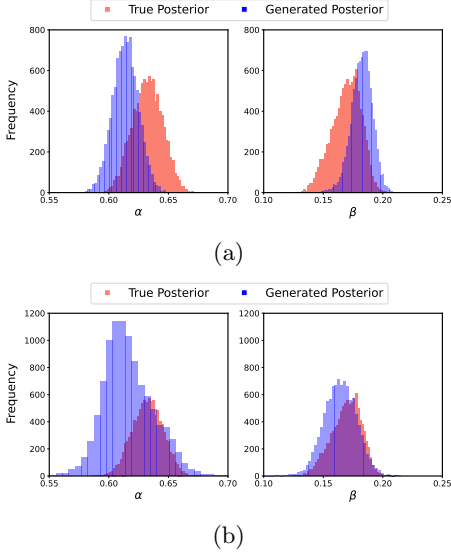


Figure 4: SIR model: true v/s estimated posterior distribution. (a) CP-VAE and (b) UP-VAE.

Figure 3 shows the recovered posterior using (a) CP-VAE and (b) UP-VAE model formulations. Both models generate samples that align closely with the true posterior, with UP-VAE exhibiting slightly better coverage of the crescent shape. Certain discrepancies, such as outliers, may be attributed to the variational lower bound in the loss function. Tables 1 and 2 present a comparative analysis using the C2ST accuracy and MMD metrics respectively. JANA and APT perform well, accurately characterizing the bimodal posterior. CP-VAE and UP-VAE closely follow, maintaining accuracy with low variance. Notably, both CP-VAE and UP-VAE are training efficient (Table 3), while demonstrating effectiveness in handling complex, unconventional posterior distributions.

4.2 The Bernoulli Generalized Linear Model

The Bernoulli Generalized Linear Model (GLM) simulates neuronal spiking behavior in response to a time-varying stimulus, driven by a set of covariates [Gonzales et al., 2020]. With a discrete time domain of $T = 100$ bins, the model produces observed data in the form $\mathbf{y} = [y_i]_{i=1}^{10}$. Each component y_i aggregates spiking activity across time intervals, capturing both overall spiking frequency and spatial patterns of neuronal activity. The model is parameterized by a vector $\boldsymbol{\theta} \in \mathbb{R}^{10}$, consisting of a scalar bias term β and an auxiliary vector $\mathbf{f} \in \mathbb{R}^9$:

$$\boldsymbol{\theta} = \begin{bmatrix} \beta \\ \mathbf{f} \end{bmatrix}, \quad \beta \sim \mathcal{N}(0, 2), \quad \mathbf{f} \sim \mathcal{N}(\mathbf{0}, (\mathbf{F}^\top \mathbf{F})^{-1}), \quad (12)$$

where the matrix \mathbf{F} enforces smoothness by penalizing second-order differences in \mathbf{f} , defined as:

$$F_{ij} = \begin{cases} 1, & j = i - 2, \\ -2, & j = i - 1, \\ 1 + \sqrt{\frac{i-1}{9}}, & j = i, \\ 0, & \text{otherwise.} \end{cases}, \quad 1 \leq i \leq 9, \quad (13)$$

For each time bin i , the binary spiking variable z_i is sampled from a Bernoulli distribution, where the spiking probability is modeled using a logistic function applied to the linear combination of covariates \mathbf{v}_i and the parameter vector, expressed as:

$$z_i \sim \text{Bernoulli}(\sigma(\mathbf{v}_i^\top \mathbf{f} + \beta)), \quad \sigma(t) = \frac{1}{1 + e^{-t}}. \quad (14)$$

Here, $\mathbf{v}_i \in \mathbb{R}^9$ represents white noise inputs (covariates) drawn from $\mathcal{N}(0, \mathbf{I})$. The design matrix $\mathbf{V} = [\mathbf{v}_i]_{i=1}^T$ aggregates these inputs over time bins T . The model computes summary statistics $\mathbf{y} \in \mathbb{R}^{10}$, where the total number of spikes is represented by $y_1 = \sum_{i=1}^T z_i$, and the remaining components, y_2, \dots, y_{10} , are spike-triggered averages of the covariates, normalized by y_1 , defined as $y_{2:10} = \frac{1}{y_1} \mathbf{V} \mathbf{z}$. The summary statistics provide a compact representation of the simulated spiking activity, capturing the overall frequency and the influence of covariates on the spiking process.

Figure 5 presents the posterior distributions of θ_1 through θ_{10} for CP-VAE and UP-VAE. In both cases, the posterior distributions align well with the true posteriors, though CP-VAE exhibits a better fit as compared to UP-VAE. CP-VAE achieves the lowest C2ST accuracy (Table 1) and MMD values (Table 2), indicating a closer match to the true posterior. UP-VAE follows closely behind on the C2ST metric, while NPE is the second-best method on the MMD metric. Both CP-VAE and UP-VAE are substantially faster to train (Table 3) showcasing efficiency and scalability for this test problem involving 10 parameters.

4.3 The SIR Model

The Susceptible-Infected-Recovered (SIR) model is a widely used mathematical framework in epidemiology for modeling the spread of infectious diseases within a population. This model tracks the evolution of the number of individuals in three distinct compartments: susceptible (S), infected (I), and recovered (R). The dynamics of disease spread are governed by a non-linear dynamical system characterized by two key parameters: the contact rate (β) and the recovery rate (γ). The model is described by the following set of ordinary differential equations:

$$\frac{d}{dt} \begin{pmatrix} S \\ I \\ R \end{pmatrix} = \begin{pmatrix} -\beta S \\ \beta S - \gamma I \\ \gamma I \end{pmatrix} \frac{I}{N}, \quad (15)$$

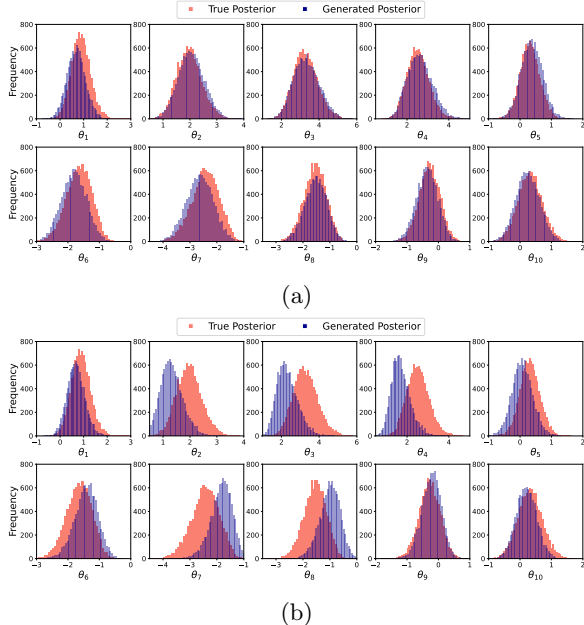


Figure 5: Bernoulli GLM: true v/s estimated posterior distribution. (a) CP-VAE and (b) UP-VAE.

where N is the total population size. The parameters are sampled as: $\beta \sim \text{LogNormal}(\log(0.4), 0.5)$ and $\gamma \sim \text{LogNormal}(\log(1/8), 0.2)$.

Figure 4 presents the posterior distributions estimated using CP-VAE and UP-VAE, respectively. Both models effectively capture complex, data-dependent relationships, resulting in accurate posterior approximations. Both CP-VAE and UP-VAE performed well on the C2ST (Table 1) and MMD metrics (Table 2), while being highly efficient (training times in Table 3).

5 Discussion

The results are now evaluated with respect to the following important considerations in SBI.

Posterior estimation accuracy: JANA and APT hold an advantage, as JANA is able to capture complex dependencies between parameters, owing to the autoregressive factorization of the joint posterior as a series of conditional distributions; while APT leverages sequential posterior refinement to enhance accuracy.

Computational efficiency: Adversarial training presents well known challenges, which reflect in relatively high training times for GATSBI. The sequential nature of APT adds computational expense over NPE and CP/UP-VAE. Autoregressive models can be computationally expensive to train and evaluate as estimating each parameter depends on previously estimated parameters – however, JANA is able to closely

match NPE’s training times for chosen hyperparameters. CP-VAE and UP-VAE are inherently simple, and do not require external summary statistics, aiding scalability and efficient training (Table 3).

Robustness/stability: GATSBI suffers from the instabilities associated with the adversarial setting (e.g., high MMD std. dev. in Table 2). JANA and APT proved to be very robust, with low std. dev. across test problems, followed by CP/UP-VAE and NPE.

Flexibility/approximating complex posteriors: APT holds an advantage over NPE due to its iterative refinement. JANA is particularly suited for posteriors with dependencies between parameters. However, the flexibility of normalizing flow based approaches (NPE, APT, JANA) is hindered by the invertibility requirement. GATSBI is suitable for complex, high-dimensional problems where other approaches may struggle and learning the posterior *implicitly* becomes important. Both CP-VAE and UP-VAE are highly flexible and adaptable with respect to the architecture.

CP-VAE v/s UP-VAE: CP-VAE’s conditional prior $p(\mathbf{z} | \mathbf{y})$ adapts to observed data, allowing flexibility and control for improved posterior accuracy. This is of particular interest in high-dimensional problems. UP-VAE’s simple Gaussian prior $p(\mathbf{z})$ allows for efficient latent space sampling, easier regularization, and a consistent latent space, leading to more stable training, making it efficient and effective for simpler problems.

The proposed CP-VAE and UP-VAE models complement existing approaches by virtue of approximating the posterior distribution in a computation-efficient manner (as evidenced in Table 3). This makes the models well-suited for challenging problems where computational efficiency is of key consideration (e.g., large number of parameters to infer, rapid model exploration, etc.). While UP-VAE uses a simpler prior, its data decoder is computationally more expensive than the conditional prior in CP-VAE, which reflects in faster training times for CP-VAE for most problems (Table 3). While we note that the training times in Table 3) can be affected by several factors including implementation and hyperparameter optimization, the comparison provides an estimate of relative computational complexity on the same hardware for reference implementations (taken from the original papers).

6 Conclusion

This paper introduces two latent variable models, CP-VAE and UP-VAE, for amortized inference in likelihood-free simulation-based inference, with a view on efficiency, scalability, interpretability and robust-

Table 1: C2ST metric for different methods across simulation budgets (mean \pm std. dev.).

Method	Two Moons			Bernoulli GLM			SIR		
Budget	10,000	20,000	30,000	10,000	20,000	30,000	10,000	20,000	30,000
GATSBI	0.7770 (\pm 0.0630)	0.6634 (\pm 0.0503)	0.7467 (\pm 0.1036)	0.9999 (\pm 0.0001)	0.9999 (\pm 0.0000)	0.9997 (\pm 0.0005)	0.9990 (\pm 0.0015)	0.9912 (\pm 0.0161)	0.9838 (\pm 0.0157)
NPE	0.5749 (\pm 0.0331)	0.5931 (\pm 0.0329)	0.5411 (\pm 0.0195)	0.9121 (\pm 0.0338)	0.8988 (\pm 0.0306)	0.8898 (\pm 0.0565)	0.8378 (\pm 0.0396)	0.9122 (\pm 0.0207)	0.9405 (\pm 0.0125)
JANA	0.5206 (\pm 0.0053)	0.5151 (\pm 0.0055)	0.5123 (\pm 0.0032)	0.9678 (\pm 0.0035)	0.9692 (\pm 0.0026)	0.9589 (\pm 0.0034)	0.8697 (\pm 0.0149)	0.9175 (\pm 0.0059)	0.9343 (\pm 0.0055)
APT	0.5189 (\pm 0.0080)	0.5202 (\pm 0.0114)	0.5147 (\pm 0.0125)	0.8404 (\pm 0.0107)	0.8328 (\pm 0.0156)	0.8353 (\pm 0.0164)	0.9433 (\pm 0.0076)	0.9434 (\pm 0.0061)	0.9457 (\pm 0.0068)
CP-VAE	0.6443 (\pm 0.0288)	0.6072 (\pm 0.0108)	0.6346 (\pm 0.0303)	0.6955 (\pm 0.0239)	0.6697 (\pm 0.0361)	0.6427 (\pm 0.0177)	0.8524 (\pm 0.0719)	0.8976 (\pm 0.0121)	0.8857 (\pm 0.0330)
UP-VAE	0.6510 (\pm 0.0310)	0.6565 (\pm 0.0364)	0.6212 (\pm 0.0252)	0.8270 (\pm 0.0249)	0.8311 (\pm 0.0216)	0.7819 (\pm 0.0692)	0.8390 (\pm 0.0378)	0.8731 (\pm 0.0482)	0.8893 (\pm 0.0317)

Table 2: MMD metric for different methods across simulation budgets (mean \pm std. dev.).

Method	Two Moons			Bernoulli GLM			SIR		
Budget	10,000	20,000	30,000	10,000	20,000	30,000	10,000	20,000	30,000
GATSBI	0.1213 (\pm 0.0650)	0.0582 (\pm 0.0122)	0.1432 (\pm 0.1161)	3.6381 (\pm 0.5428)	4.8299 (\pm 0.6825)	3.9965 (\pm 1.8510)	2.9470 (\pm 0.4891)	2.7502 (\pm 0.7268)	2.1466 (\pm 0.5625)
NPE	0.0254 (\pm 0.0025)	0.0241 (\pm 0.0099)	0.0125 (\pm 0.0045)	1.0371 (\pm 0.1830)	0.9379 (\pm 0.1001)	0.8675 (\pm 0.1945)	0.6611 (\pm 0.2236)	1.0312 (\pm 0.1255)	1.1903 (\pm 0.1007)
JANA	0.0060 (\pm 0.0013)	0.0068 (\pm 0.0017)	0.0047 (\pm 0.0009)	3.3232 (\pm 0.0932)	3.1488 (\pm 0.0280)	2.9010 (\pm 0.0878)	0.8495 (\pm 0.1254)	1.1077 (\pm 0.0336)	1.1421 (\pm 0.0392)
APT	0.0073 (\pm 0.0030)	0.0069 (\pm 0.0030)	0.0037 (\pm 0.0012)	0.7383 (\pm 0.0853)	0.4944 (\pm 0.0663)	0.5808 (\pm 0.0539)	1.1003 (\pm 0.0712)	1.1093 (\pm 0.0311)	1.1291 (\pm 0.0481)
CP-VAE	0.0382 (\pm 0.0110)	0.0369 (\pm 0.0088)	0.0276 (\pm 0.0050)	0.1966 (\pm 0.1375)	0.1557 (\pm 0.0663)	0.0942 (\pm 0.0547)	0.8792 (\pm 0.3327)	1.0158 (\pm 0.0566)	0.9990 (\pm 0.1923)
UP-VAE	0.0736 (\pm 0.0097)	0.0795 (\pm 0.0151)	0.0544 (\pm 0.0150)	1.5420 (\pm 0.4930)	1.4748 (\pm 0.2623)	1.1160 (\pm 0.7496)	0.5168 (\pm 0.1193)	0.6884 (\pm 0.2044)	0.6487 (\pm 0.1087)

Table 3: Training time for different methods across simulation budgets (mean \pm std. dev. in minutes).

Method	Two Moons			Bernoulli GLM			SIR		
Budget	10,000	20,000	30,000	10,000	20,000	30,000	10,000	20,000	30,000
GATSBI	117.67 (\pm 2.43)	164.90 (\pm 57.10)	249.50 (\pm 105.05)	118.62 (\pm 0.18)	179.69 (\pm 49.96)	253.48 (\pm 113.38)	227.16 (\pm 1.44)	241.24 (\pm 7.58)	250.47 (\pm 2.22)
NPE	7.04 (\pm 0.21)	14.21 (\pm 0.04)	20.95 (\pm 0.37)	12.17 (\pm 0.17)	24.96 (\pm 0.64)	37.43 (\pm 0.22)	20.10 (\pm 5.45)	29.62 (\pm 3.74)	44.92 (\pm 9.24)
JANA	5.66 (\pm 0.10)	9.48 (\pm 0.12)	14.34 (\pm 0.11)	7.14 (\pm 0.05)	12.23 (\pm 0.07)	19.00 (\pm 0.19)	22.98 (\pm 0.32)	39.17 (\pm 2.48)	61.89 (\pm 5.41)
APT	90.31 (\pm 8.99)	186.17 (\pm 13.79)	268.28 (\pm 32.88)	101.39 (\pm 7.89)	197.30 (\pm 9.32)	267.38 (\pm 21.93)	40.15 (\pm 3.90)	73.74 (\pm 6.25)	112.51 (\pm 2.51)
CP-VAE	2.23 (\pm 0.81)	3.75 (\pm 0.80)	4.99 (\pm 0.83)	1.76 (\pm 0.27)	3.64 (\pm 0.14)	4.93 (\pm 0.47)	2.77 (\pm 0.40)	6.06 (\pm 1.09)	8.68 (\pm 0.83)
UP-VAE	1.98 (\pm 0.33)	3.27 (\pm 0.58)	5.35 (\pm 1.82)	2.10 (\pm 0.50)	4.43 (\pm 0.61)	6.57 (\pm 1.04)	4.44 (\pm 0.88)	6.71 (\pm 1.97)	9.60 (\pm 1.66)

ness. The proposed models are validated against state-of-the-art normalizing flow and adversarial training-based approaches on benchmark test problems. Both CP-VAE and UP-VAE deliver comparable performance to the state-of-the-art while being highly computation efficient and scalable. Future enhancements could involve integrating more sophisticated architectures (e.g., Convolutional Neural Networks) to better capture spatial and temporal dependencies within the

data. Exploring diverse prior distributions, such as truncated Gaussian priors, may further improve the models' ability to approximate complex posteriors.

Acknowledgements

The computations/data handling were enabled by the Berzelius resource provided by the Knut and Alice Wallenberg Foundation at the National Super-

computer Centre and by the National Academic Infrastructure for Supercomputing in Sweden (NAISS) at Chalmers e-Commons at Chalmers, and Uppsala Multidisciplinary Center for Advanced Computational Science (UPPMAX) at Uppsala University, partially funded by the Swedish Research Council through grant agreement nos. 2022-06725 and 2018-05973. AH and PS acknowledge support from the Swedish Research Council through grant agreement nos. 2023-05167 and 2023-05593 respectively.

References

- Martin Arjovsky and Leon Bottou. Towards principled methods for training generative adversarial networks, 2022.
- Martin Arjovsky, Soumith Chintala, and Léon Bottou. Wasserstein generative adversarial networks. In *International conference on machine learning*, pages 214–223. PMLR, 2017.
- Kyle Cranmer, Johann Brehmer, and Gilles Louppe. The frontier of simulation-based inference. *Proceedings of the National Academy of Sciences*, 117(48):30055–30062, 2020.
- Jerome H Friedman. On multivariate goodness-of-fit and two-sample testing. *Statistical Problems in Particle Physics, Astrophysics, and Cosmology*, 1:311, 2003.
- Manuel Glöckler, Michael Deistler, and Jakob H. Macke. Variational methods for simulation-based inference. In *International Conference on Learning Representations*, 2022. URL <https://openreview.net/forum?id=kZ0UYdhqkNY>.
- Manuel Gloeckler, Michael Deistler, Christian Dietrich Weillbach, Frank Wood, and Jakob H Macke. All-in-one simulation-based inference. In *Forty-first International Conference on Machine Learning*.
- Pedro J Gonzalves, Jan-Matthis Lueckmann, Michael Deistler, Marcel Nonnenmacher, Kaan Öcal, Giacomo Bassetto, Chaitanya Chintaluri, William F Podlaski, Sara A Haddad, Tim P Vogels, David S Greenberg, and Jakob H Macke. Training deep neural density estimators to identify mechanistic models of neural dynamics. *eLife*, 9:e56261, sep 2020. ISSN 2050-084X. doi: 10.7554/eLife.56261. URL <https://doi.org/10.7554/eLife.56261>.
- David Greenberg, Marcel Nonnenmacher, and Jakob Macke. Automatic posterior transformation for likelihood-free inference. In *International Conference on Machine Learning*, pages 2404–2414. PMLR, 2019.
- Joeri Hermans, Volodimir Begy, and Gilles Louppe. Likelihood-free mcmc with amortized approximate ratio estimators. In *International conference on machine learning*, pages 4239–4248. PMLR, 2020.
- Oleg Ivanov, Michael Figurnov, and Dmitry Vetrov. Variational autoencoder with arbitrary conditioning. In *International Conference on Learning Representations*, 2019. URL <https://openreview.net/forum?id=SyxtJh0qYm>.
- Michael I Jordan, Zoubin Ghahramani, Tommi S Jaakkola, and Lawrence K Saul. An introduction to variational methods for graphical models. *Machine learning*, 37(2):183–233, 1999. doi: 10.1023/A:1007665907178.
- Diederik P. Kingma and Max Welling. Auto-encoding variational bayes. In *2nd International Conference on Learning Representations, ICLR 2014*, 2014. URL <http://arxiv.org/abs/1312.6114v10>.
- Alexander Lavin, Hector Zenil, Brooks Paige, David C. Krakauer, Justin Emile Gottschlich, Timothy G. Mattson, Anima Anandkumar, Sanjay Choudry, Kamil Rocki, Atilim Gunecs Baydin, Carina E. A. Prunkl, Olexandr Isayev, Erik J Peterson, Peter Leonard McMahon, Jakob H. Macke, Kyle Cranmer, Jiaxin Zhang, Haruko Murakami Wainwright, Adi Hanuka, Manuela M. Veloso, Samuel A. Assefa, Stephan Zheng, and Avi Pfeffer. Simulation intelligence: Towards a new generation of scientific methods. *ArXiv*, abs/2112.03235, 2021. URL <https://api.semanticscholar.org/CorpusID:244909059>.
- Jan-Matthis Lueckmann, Pedro J Goncalves, Giacomo Bassetto, Kaan Öcal, Marcel Nonnenmacher, and Jakob H Macke. Flexible statistical inference for mechanistic models of neural dynamics. In *Advances in Neural Information Processing Systems*, volume 30. Curran Associates, Inc., 2017. URL https://proceedings.neurips.cc/paper_files/paper/2017/file/addfa9b7e234254d26e9c7f2af1005cb-Paper.pdf.
- Jan-Matthis Lueckmann, Jan Boelts, David Greenberg, Pedro Goncalves, and Jakob Macke. Benchmarking simulation-based inference. In *Proceedings of The 24th International Conference on Artificial Intelligence and Statistics*, volume 130 of *Proceedings of Machine Learning Research*, pages 343–351. PMLR, 13–15 Apr 2021.
- George Papamakarios and Iain Murray. Fast ε -free inference of simulation models with bayesian conditional density estimation. *Advances in neural information processing systems*, 29, 2016.

- Stefan T Radev, Marvin Schmitt, Valentin Pratz, Umberto Picchini, Ullrich Köthe, and Paul-Christian Bürkner. Jana: Jointly amortized neural approximation of complex bayesian models. In *Uncertainty in Artificial Intelligence*, pages 1695–1706. PMLR, 2023a.
- Stefan T. Radev, Marvin Schmitt, Lukas Schumacher, Lasse Elsemüller, Valentin Pratz, Yannik Schälte, Ullrich Köthe, and Paul-Christian Bürkner. BayesFlow: Amortized Bayesian workflows with neural networks. *Journal of Open Source Software*, 8(89):5702, 2023b.
- Poornima Ramesh, Jan-Matthis Lueckmann, Jan Boelts, Álvaro Tejero-Cantero, David S. Greenberg, Pedro J. Goncalves, and Jakob H. Macke. GATSBI: Generative adversarial training for simulation-based inference. In *International Conference on Learning Representations*, 2022. URL <https://openreview.net/forum?id=kR1hC6j48Tp>.
- Danilo Rezende and Shakir Mohamed. Variational inference with normalizing flows. In *International conference on machine learning*, pages 1530–1538. PMLR, 2015.
- Ivaxi Sheth and Samira Ebrahimi Kahou. Auxiliary losses for learning generalizable concept-based models. In *Proceedings of the 37th International Conference on Neural Information Processing Systems*, NeurIPS '23, Red Hook, NY, USA, 2024. Curran Associates Inc.
- Scott A Sisson, Yanan Fan, and Mark Beaumont. *Handbook of approximate Bayesian computation*. CRC press, 2018.
- Kihyuk Sohn, Honglak Lee, and Xinchen Yan. Learning structured output representation using deep conditional generative models. *Advances in neural information processing systems*, 28, 2015.
- Daniel Ward, Patrick Cannon, Mark Beaumont, Matteo Fasiolo, and Sebastian Schmon. Robust neural posterior estimation and statistical model criticism. *Advances in Neural Information Processing Systems*, 35:33845–33859, 2022.
- Samuel Wiqvist, Jes Frellsen, and Umberto Picchini. Sequential neural posterior and likelihood approximation, 2021.
- Andrew Zammit-Mangion, Matthew Sainsbury-Dale, and Raphaël Huser. Neural methods for amortised parameter inference. *arXiv preprint arXiv:2404.12484*, 2024.

Appendix/Supplementary Material

1 Derivation of the Loss Function for CP-VAE Model

To derive the loss function for the CP-VAE model, we begin by referencing the intractable formulation presented in Section 3.1, Equation (6) of the main text, to arrive at a tractable approximation. The original loss function is defined as:

$$\mathcal{L}(\boldsymbol{\theta}, \mathbf{y}; \psi) = \underbrace{D_{KL}(q_\psi(\mathbf{z} | \mathbf{y}, \boldsymbol{\theta}) \| p(\mathbf{z} | \mathbf{y}))}_{\text{Term 1}} - \underbrace{\mathbb{E}_{\mathbf{z} \sim q_\psi(\mathbf{z} | \mathbf{y}, \boldsymbol{\theta})}[\log p(\boldsymbol{\theta} | \mathbf{y}, \mathbf{z})]}_{\text{Term 2}}, \quad (1)$$

where, $\boldsymbol{\theta}$ represents the parameter vector, \mathbf{y} is the observed data, and ψ consists of the parameters of the variational distribution.

To ensure tractability of the Kullback-Leibler (KL) divergence term, $D_{KL}(q_\psi(\mathbf{z} | \mathbf{y}, \boldsymbol{\theta}) \| p(\mathbf{z} | \mathbf{y}))$, we assume both the variational distribution $q_\psi(\mathbf{z} | \mathbf{y}, \boldsymbol{\theta}) \sim \mathcal{N}(\boldsymbol{\mu}_q, \boldsymbol{\Sigma}_q)$ and the prior $p(\mathbf{z} | \mathbf{y}) \sim \mathcal{N}(\boldsymbol{\mu}_y, \boldsymbol{\Sigma}_y)$ to be multivariate Gaussian distributions with diagonal covariance matrices. The diagonal structure of the covariance matrices ensures that only the variances of individual components are modeled, eliminating off-diagonal correlations. These distributions are parameterized by neural networks, with $\boldsymbol{\mu}_q$, $\boldsymbol{\Sigma}_q$, $\boldsymbol{\mu}_y$, and $\boldsymbol{\Sigma}_y$ being functions of the network parameters ψ and ϕ , respectively. This allows for closed-form computation of the KL divergence between the variational distribution and the prior, given by:

$$D_{KL}(\mathcal{N}(\boldsymbol{\mu}_q, \boldsymbol{\Sigma}_q) \| \mathcal{N}(\boldsymbol{\mu}_y, \boldsymbol{\Sigma}_y)) = \frac{1}{2} \left(\log \frac{|\boldsymbol{\Sigma}_y|}{|\boldsymbol{\Sigma}_q|} - d + \text{tr}(\boldsymbol{\Sigma}_y^{-1} \boldsymbol{\Sigma}_q) + (\boldsymbol{\mu}_y - \boldsymbol{\mu}_q)^\top \boldsymbol{\Sigma}_y^{-1} (\boldsymbol{\mu}_y - \boldsymbol{\mu}_q) \right), \quad (2)$$

where d represents the dimensionality of the latent variable \mathbf{z} . To approximate the second term, $\mathbb{E}_{\mathbf{z} \sim q_\psi(\mathbf{z} | \mathbf{y}, \boldsymbol{\theta})}[\log p(\boldsymbol{\theta} | \mathbf{y}, \mathbf{z})]$, we again assume, that $p(\boldsymbol{\theta} | \mathbf{y}, \mathbf{z}) = \mathcal{N}(\boldsymbol{\mu}_\theta, \boldsymbol{\Sigma}_\theta)$ follows a multivariate normal distribution for computational tractability, where the mean $\boldsymbol{\mu}_\theta$ and covariance $\boldsymbol{\Sigma}_\theta$ are parameterized by a neural network with parameters δ . The probability density function of this distribution is given by:

$$p(\boldsymbol{\theta} | \mathbf{y}, \mathbf{z}) = \frac{1}{(2\pi)^{k/2} |\boldsymbol{\Sigma}_\theta|^{1/2}} \exp \left(-\frac{1}{2} (\boldsymbol{\theta} - \boldsymbol{\mu}_\theta)^\top \boldsymbol{\Sigma}_\theta^{-1} (\boldsymbol{\theta} - \boldsymbol{\mu}_\theta) \right). \quad (3)$$

Taking the logarithm of both sides in (3), we obtain:

$$\log p(\boldsymbol{\theta} | \mathbf{y}, \mathbf{z}) = -\frac{1}{2} \left(k \log(2\pi) + \log |\boldsymbol{\Sigma}_\theta| + (\boldsymbol{\theta} - \boldsymbol{\mu}_\theta)^\top \boldsymbol{\Sigma}_\theta^{-1} (\boldsymbol{\theta} - \boldsymbol{\mu}_\theta) \right). \quad (4)$$

Since the determinant of the diagonal covariance matrix is given by $|\boldsymbol{\Sigma}_\theta| = \prod_{i=1}^k \sigma_{\theta_i}^2$, we can simplify $\log |\boldsymbol{\Sigma}_\theta|$ as $\log |\boldsymbol{\Sigma}_\theta| = \log \left(\prod_{i=1}^k \sigma_{\theta_i}^2 \right) = 2 \sum_{i=1}^k \log \sigma_{\theta_i}$. Substituting this simplification back into (4) and taking the expectation with respect to $\mathbf{z} \sim q_\psi(\mathbf{z} | \mathbf{y}, \boldsymbol{\theta})$ on both sides, we obtain:

$$\mathbb{E}_{\mathbf{z} \sim q_\psi} [\log p(\boldsymbol{\theta} | \mathbf{y}, \mathbf{z})] = -\frac{1}{2} \left(k \log(2\pi) + 2 \sum_{i=1}^k \log \sigma_{\theta_i} + \mathbb{E}_{\mathbf{z} \sim q_\psi} [(\boldsymbol{\theta} - \boldsymbol{\mu}_\theta)^\top \boldsymbol{\Sigma}_\theta^{-1} (\boldsymbol{\theta} - \boldsymbol{\mu}_\theta)] \right). \quad (5)$$

Given that $\boldsymbol{\Sigma}_\theta$ is a diagonal matrix, the quadratic form simplifies to a sum of squares. The expectation over N data points can then be expressed as:

$$\mathbb{E}_{\mathbf{z} \sim q_\psi} [(\boldsymbol{\theta} - \boldsymbol{\mu}_\theta)^\top \boldsymbol{\Sigma}_\theta^{-1} (\boldsymbol{\theta} - \boldsymbol{\mu}_\theta)] = \mathbb{E}_{\mathbf{z} \sim q_\psi} \left[\sum_{i=1}^k \frac{(\theta_i - \mu_{\theta_i})^2}{\sigma_{\theta_i}^2} \right] = \frac{1}{N} \sum_{j=1}^N \sum_{i=1}^k \frac{(\theta_{i,j} - \mu_{\theta_i})^2}{\sigma_{\theta_i}^2}. \quad (6)$$

The term $k \log(2\pi)$ is constant, and can be excluded from the optimization, allowing (5) to be written as:

$$\mathbb{E}_{\mathbf{z} \sim q_\psi} [\log p(\boldsymbol{\theta} | \mathbf{y}, \mathbf{z})] \approx - \sum_{i=1}^k \log \sigma_{\theta_i} - \frac{1}{2N} \sum_{j=1}^N \sum_{i=1}^k \frac{(\theta_{i,j} - \mu_{\theta_i})^2}{\sigma_{\theta_i}^2}. \quad (7)$$

Substituting (2) and (7) into (1), we obtain the tractable loss function:

$$\begin{aligned} \mathcal{L}(\boldsymbol{\theta}, \mathbf{y}; \psi, \phi, \delta) = & \frac{1}{2} \left(\log \frac{|\boldsymbol{\Sigma}_{\mathbf{y}}|}{|\boldsymbol{\Sigma}_q|} - k + \text{tr}(\boldsymbol{\Sigma}_{\mathbf{y}}^{-1} \boldsymbol{\Sigma}_q) + (\boldsymbol{\mu}_{\mathbf{y}} - \boldsymbol{\mu}_q)^\top \boldsymbol{\Sigma}_{\mathbf{y}}^{-1} (\boldsymbol{\mu}_{\mathbf{y}} - \boldsymbol{\mu}_q) \right) \\ & + \sum_{i=1}^k \log \sigma_{\theta_i} + \frac{1}{2N} \sum_{j=1}^N \sum_{i=1}^k \frac{(\theta_{i,j} - \mu_{\theta_i})^2}{\sigma_{\theta_i}^2}. \end{aligned} \quad (8)$$

We now aim to minimize Equation 8 by learning the parameters ψ , ϕ , and δ through stochastic gradient methods.

2 Derivation of the Loss Function for UP-VAE Model

To obtain a tractable form of the loss function for the UP-VAE model, we begin with the expression outlined in Equation (10) of Section 3.2 in the main text:

$$\mathcal{L}(\boldsymbol{\theta}, \mathbf{y}; \psi) = \underbrace{D_{KL}(q_\psi(\mathbf{z} | \mathbf{y}, \boldsymbol{\theta}) || p(\mathbf{z}))}_{\text{Term 1}} - \underbrace{\mathbb{E}_{\mathbf{z} \sim q_\psi(\mathbf{z} | \mathbf{y}, \boldsymbol{\theta})} [\log p(\boldsymbol{\theta} | \mathbf{y}, \mathbf{z})]}_{\text{Term 2}} - \underbrace{\mathbb{E}_{\mathbf{z} \sim q_\psi(\mathbf{z} | \mathbf{y}, \boldsymbol{\theta})} [\log p(\mathbf{y} | \mathbf{z})]}_{\text{Term 3}}. \quad (9)$$

We approximate Terms 2 and 3 using a formulation akin to that in Equation 7. We approximate Term 2, $\mathbb{E}_{\mathbf{z} \sim q_\psi} [\log p(\boldsymbol{\theta} | \mathbf{y}, \mathbf{z})]$, by assuming that $p(\boldsymbol{\theta} | \mathbf{y}, \mathbf{z})$ is a multivariate Gaussian distribution characterized by mean $\boldsymbol{\mu}_\theta$ and covariance $\boldsymbol{\Sigma}_\theta$, with k_θ denoting the dimensionality of $\boldsymbol{\theta}$. These parameters are learned using a neural network parameterized by ϕ . This assumption yields the following expression:

$$\mathbb{E}_{\mathbf{z} \sim q_\psi} [\log p(\boldsymbol{\theta} | \mathbf{y}, \mathbf{z})] \approx - \sum_{i=1}^{k_\theta} \log \sigma_{\theta_i} - \frac{1}{2N} \sum_{j=1}^N \sum_{i=1}^{k_\theta} \frac{(\theta_{i,j} - \mu_{\theta_i})^2}{\sigma_{\theta_i}^2}. \quad (10)$$

Similarly, for Term 3, we approximate $\mathbb{E}_{\mathbf{z} \sim q_\psi} [\log p(\mathbf{y} | \mathbf{z})]$ by assuming that $p(\mathbf{y} | \mathbf{z}) \sim \mathcal{N}(\mathbf{y}; \boldsymbol{\mu}_{\mathbf{y}}, \boldsymbol{\Sigma}_{\mathbf{y}})$, with $k_{\mathbf{y}}$ represents the dimensionality of \mathbf{y} . The parameters of this distribution are learned by a neural network parameterized by δ . From Equation (7), this can be expressed as:

$$\mathbb{E}_{\mathbf{z} \sim q_\psi} [\log p(\mathbf{y} | \mathbf{z})] \approx - \sum_{i=1}^{k_{\mathbf{y}}} \log \sigma_{\mathbf{y}_i} - \frac{1}{2N} \sum_{j=1}^N \sum_{i=1}^{k_{\mathbf{y}}} \frac{(y_{i,j} - \mu_{\mathbf{y}_i})^2}{\sigma_{\mathbf{y}_i}^2}. \quad (11)$$

To handle the KL divergence (Term 1), we assume a standard normal prior $p(\mathbf{z}) = \mathcal{N}(\mathbf{0}, \mathbf{I})$, where $\mathbf{0}$ is the zero mean vector and \mathbf{I} is the identity covariance matrix. This simplifies the computation of the KL divergence between the variational distribution $q_\psi(\mathbf{z} | \mathbf{y}, \boldsymbol{\theta})$, modeled as a Gaussian with mean $\boldsymbol{\mu}_q$ and covariance $\boldsymbol{\Sigma}_q$, and the prior, allowing for a closed-form solution:

$$D_{KL}(\mathcal{N}(\boldsymbol{\mu}_q, \boldsymbol{\Sigma}_q) || \mathcal{N}(\mathbf{0}, \mathbf{I})) = \frac{1}{2} \left(-\log |\boldsymbol{\Sigma}_q| - k_{\mathbf{z}} + \text{tr}(\boldsymbol{\Sigma}_q) + \boldsymbol{\mu}_q^\top \boldsymbol{\mu}_q \right), \quad (12)$$

where $k_{\mathbf{z}}$ represents the dimensionality of the latent variable \mathbf{z} . Substituting (10), (11) and (12) into (9), the final expression for the loss function is as follows:

$$\begin{aligned} \mathcal{L}(\boldsymbol{\theta}, \mathbf{y}; \psi, \phi, \delta) = & \frac{1}{2} \left(-\log |\boldsymbol{\Sigma}_q| - k_{\mathbf{z}} + \text{tr}(\boldsymbol{\Sigma}_q) + \boldsymbol{\mu}_q^\top \boldsymbol{\mu}_q \right) + \sum_{i=1}^{k_\theta} \log \sigma_{\theta_i} + \frac{1}{2N} \sum_{j=1}^N \sum_{i=1}^{k_\theta} \frac{(\theta_{i,j} - \mu_{\theta_i})^2}{\sigma_{\theta_i}^2} \\ & + \sum_{i=1}^{k_{\mathbf{y}}} \log \sigma_{\mathbf{y}_i} + \frac{1}{2N} \sum_{j=1}^N \sum_{i=1}^{k_{\mathbf{y}}} \frac{(y_{i,j} - \mu_{\mathbf{y}_i})^2}{\sigma_{\mathbf{y}_i}^2}. \end{aligned} \quad (13)$$

Here we aim to optimize the parameters ψ , ϕ , and δ , which represent the neural network parameters associated with the variational distribution and the two decoder models.

3 SBI Benchmarking Problems

The Simulation-Based Inference (SBI) benchmarking test problems offer a standardized set of tasks to evaluate various inference methods. These problems span a range of dimensionalities and complexities, ensuring a comprehensive assessment across diverse scenarios. Each problem is characterized by its unique prior, simulator, and data dimensionality, enabling a comprehensive evaluation of inference methods under different conditions. Every task includes 10 observations with known ground truth posteriors and their corresponding true generating parameters. An overview of the benchmarking problems are presented in Table 1. For in-depth details about the mathematical formulations of each benchmarking test, we direct the reader to [Lueckmann et al., 2021].

Table 1: An overview of the benchmark test problems.

No.	Benchmark	Dimensions*	Prior	Description
1	Gaussian Linear	(10, 10)	$\mathcal{N}(0, 0.1\mathbf{I})$	Simple Gaussian inference with fixed covariance
2	Gaussian Linear Uniform	(10, 10)	$\mathcal{U}(-1, 1)$	Uniform prior with fixed covariance
3	SLCP	(5, 8)	$\mathcal{U}(-3, 3)$	Complex posterior with nonlinear functions of θ
4	SLCP with Distractors	(5, 100)	$\mathcal{U}(-3, 3)$	High-dimensional input with uninformative distractors
5	Bernoulli GLM	(10, 10)	$\mathcal{N}(0, 2)$	Generalized Linear Model with Bernoulli observations
6	Bernoulli GLM Raw	(10, 100)	$\mathcal{N}(0, 2)$	Raw observations for Bernoulli GLM process
7	Gaussian Mixture	(2, 2)	$\mathcal{U}(-10, 10)$	Mixture of two Gaussians with different covariances
8	Two Moons	(2, 2)	$\mathcal{U}(-1, 1)$	Bimodal distribution with local and global structures
9	SIR	(2, 10)	$\beta \sim \log \mathcal{N}(\log(0.4), 0.5)$ $\gamma \sim \log \mathcal{N}(\log(1/8), 0.2)$	Epidemiological model with SIR dynamics
10	Lotka-Volterra	(4, 20)	$\alpha \sim \log \mathcal{N}(-0.125, 0.5)$ $\beta \sim \log \mathcal{N}(-3, 0.5)$ $\gamma \sim \log \mathcal{N}(-0.125, 0.5)$ $\delta \sim \log \mathcal{N}(-3, 0.5)$	Ecological model with interacting species

*Dimensions are in the (θ, \mathbf{y}) format.

4 Stabilizing the training process

In both CP-VAE and UP-VAE models, we approximate the loss using a multivariate distribution with both mean and variance. Unbounded variance—where σ^2 becomes excessively small or large—can lead to numerical instabilities, disrupting training. To improve stability, ? suggest the ExpLin parameterization, which combines

exponential and linear functions:

$$\sigma(p) = \begin{cases} \exp(p) & \text{if } p \leq 0, \\ p + 1 & \text{if } p > 0. \end{cases} \quad (14)$$

This approach ensures positive variance for small values of p , while preventing excessive growth for large values. It thus balances stability and reduces the risk of training disruptions. Additionally, we use the Sigmoid-Based UpBounded parameterization in the decoder to further control variance. The UpBounded parameterization with sigmoid function is defined as:

$$\sigma(p) = \alpha + (\omega - \alpha) \cdot \text{sigmoid}(p). \quad (15)$$

This formulation smoothly caps the variance within the range $[\alpha, \omega]$, ensuring controlled decoder output variance. ExpLin effectively handles the variance in the latent space, while the sigmoid-based parameterization keeps the decoder’s variance stable. This approach reduces the likelihood of training disruptions and improves overall model stability.

5 Hyperparameters

In this section, we outline the hyperparameters used for all the methods considered in the paper. We consider fixed simulation budgets of $\{10,000; 20,000; 30,000\}$ for all test problems to evaluate various methods. The observed data and reference posterior samples come from the pre-generated datasets provided by the `sbibm` library [Lueckmann et al., 2021], allowing us to directly load both the observed data and the corresponding reference posterior for consistent and accurate benchmarking across different tasks. An alternate implementation is also available in BayesFlow framework [Radev et al., 2023b]. We consider the first observation for all problems except the SIR model. For the SIR model, we faced issues with the observed data not aligning with the true parameters when transitioning from `sbibm` to BayesFlow. We tested this by generating 10,000 samples from the simulator using the same parameters provided in the `sbibm` SIR dataset, confirming the misalignment between the observed data and the true parameters. To address this, we considered the true parameter from `sbibm` and generated the observed data by evaluating the simulator in BayesFlow. For details on the reference posterior generation process, the reader is referred to as to Section B.1 of the supplementary material of the `sbibm` paper.

5.1 CP-VAE

In this configuration, common parameters are applied uniformly across all problems, with specific architectures detailed in Table 2. Each network — $q_\phi(\mathbf{z} \mid \mathbf{y}, \boldsymbol{\theta})$, $p(\mathbf{z} \mid \mathbf{y})$, and $p(\boldsymbol{\theta} \mid \mathbf{y}, \mathbf{z})$ — is designed to approximate a multivariate distribution, outputting both a mean and variance vector. Specifically, the last layer in $q_\phi(\mathbf{z} \mid \mathbf{y}, \boldsymbol{\theta})$ and $p(\mathbf{z} \mid \mathbf{y})$ outputs a vector of size $2 \times \text{latent_dim}$, while the last layer in $p(\boldsymbol{\theta} \mid \mathbf{y}, \mathbf{z})$ outputs a vector of size $2 \times \text{theta_dim}$. Leaky ReLU activation functions with a negative slope of 0.1 are used throughout, with a learning rate of 5×10^{-4} , except for the Lotka-Volterra model, which uses 10^{-4} , and the AdamW optimizer [?]. Models are trained with a batch size of 32 (except SLCP, which uses 16, and Lotka-Volterra, which uses 128) for 1,000 epochs, with early stopping triggered if validation performance does not improve for 20 consecutive epochs. Both $\boldsymbol{\theta}$ and the data are normalized using standard scaling, and gradient clipping is set to 3.0. The latent dimension is equal to the $\boldsymbol{\theta}$ dimension, except for the Gaussian Linear and GLM raw models, which use 5, Lotka-Volterra uses 8, SLCP uses 4, SLCP with Distractors uses 8, and Gaussian Linear uses 5. Kaiming normal initialization is used for weights. For each simulation budget, 90% of the data is used for training, with the remaining 10% reserved for validation.

Table 2: Architectural details of the CP-VAE model.

Problem	$q_\phi(\mathbf{z} \mid \mathbf{y}, \boldsymbol{\theta})$	$p(\mathbf{z} \mid \mathbf{y})$	$p(\boldsymbol{\theta} \mid \mathbf{y}, \mathbf{z})$
Gaussian Linear	(64, 64, 64)	(64, 64)	(64, 64, 64)
Gaussian Linear Uniform	(64, 64, 64)	(64,64)	(64,64,64)
SLCP	(200, 200, 200)	(64, 64)	(200,200)
SLCP with Distractors	(200,200,200)	(64,64)	(200,200,200)
Bernoulli GLM	(128,128,128)	(128,128)	(128,128,128)
Bernoulli GLM Raw	(256,256,256,256)	(128,128)	(256,256,256,256)
Gaussian Mixture	(64, 64, 64)	(64, 64)	(64, 64, 64)
Two Moons	(128, 128, 128)	(128, 128)	(128, 128, 128)
SIR	(100,100)	(100,100)	(100,100,100)
Lotka-Volterra	(128,128,128,128)	(64,64)	(128,128,128, 128)

5.2 UP-VAE

Building on the CP-VAE model, the UP-VAE model retains several core hyperparameters while incorporating key enhancements. Shared parameters include a learning rate of 5×10^{-4} , except for the Lotka-Volterra (LV) model, which uses 10^{-4} , a batch size of 32 (except Two Moons, which uses 50, and LV, which uses 128), and 1,000 training epochs with early stopping after 20 epochs of no improvement. Standard scaling, gradient clipping (set to 3.0), Kaiming normal initialization, and a 90-10 train-validation split are consistently applied. In the UP-VAE model, the networks $q_\phi(\mathbf{z} \mid \mathbf{y}, \boldsymbol{\theta})$, $p(\boldsymbol{\theta} \mid \mathbf{y}, \mathbf{z})$, and $p(\mathbf{y} \mid \mathbf{z})$ approximate multivariate distributions, producing both mean and variance vectors. The final layers of these networks consist of separate fully connected layers for the mean (μ) and variance (σ^2), outputting vectors of size corresponding to the dimensions of \mathbf{z} , $\boldsymbol{\theta}$, and \mathbf{y} , respectively. The loss function weights are adjusted, with data reconstruction set to 0.2, theta loss to 0.4, and KL divergence to 0.4, reflecting the model’s primary focus on the theta decoder and constraining the latent space. Specific architectures for these components across different problems are detailed in Table 3.

Table 3: Architectural details for the UP-VAE model.

Problem	$q_\phi(\mathbf{z} \mid \mathbf{y}, \boldsymbol{\theta})$	$p(\boldsymbol{\theta} \mid \mathbf{y}, \mathbf{z})$	$p(\mathbf{y} \mid \mathbf{z})$
Gaussian Linear	(64, 64, 64)	(64, 64, 64)	(64, 64, 64)
Gaussian Linear Uniform	(64, 64, 64)	(64, 64, 64)	(64, 64, 64)
SLCP	(200,200,200)	(200,200,200)	(200,200,200)
SLCP with Distractors	(200,100,50,25)	(200,100,50, 25)	(128,128,128)
Bernoulli GLM	(128,128,128)	(128,128,128)	(128,128,128)
Bernoulli GLM Raw	(128,128,128, 128)	(128,128,128, 128)	(128,128,128, 128)
Gaussian Mixture	(64, 64, 64)	(64, 64, 64)	(64, 64, 64)
Two Moons	(256,128,64)	(256,128,64)	(256,128,64)
SIR	(100,100,100)	(100,100,100)	(100,100,100)
Lotka-Volterra	(128,128,128,128)	(128,128,128)	(128,128,128)

5.3 JANA

We use the hyperparameters provided in the supplementary text of the original paper [Radev et al., 2023a].

5.4 NPE

The original paper on Neural Posterior Estimation (NPE) does not test the method on all the SBI benchmarking problems. However, the `sbibm` paper has evaluated NPE on all 10 benchmarking problems [Lueckmann et al., 2021]. As reported in Appendix H of the `sbibm` paper, Neural Spline Flows (NSF) are generally a better choice of density estimator than Masked Autoregressive Flows (MAF), which was originally recommended in the NPE

paper. Therefore, we use the default NSF from `sbi` [?] package as the density estimator for all the problems here. We use the SBI toolbox to implement Neural Posterior Estimation (NPE), which is equivalent to running the Sequential NPE (SNPE) class for a single round of simulation and training. NSF uses five flow transformations, two residual blocks of 50 hidden units each with ReLU non-linearity, and 10 bins as reported in section A5 of the supplementary of `sbibm` paper.

For problems involving time series data, it is recommended to use a summary network for NPE [?]. Following this, we modify and optimize the standard `CNNEmbedding` provided by the `sbi` package. This network transforms the data into summary statistics with the dimensionality matching the parameters, which is 4 for the Lotka-Volterra (LV) test problem and 2 for the Susceptible-Infectious-Recovered (SIR) test problem. For LV, the CNN architecture includes two 1D convolutional layers with 64 output channels each, followed by two fully connected layers with 128 units each. For SIR, the CNN has two 1D convolutional layers with 32 output channels each, followed by fully connected layers with 64 units each. For both problems, we use MaxPooling layers of size 2 after each CNN layer and ReLU activation throughout. We train the density estimator for 200 epochs with the default learning rate of 0.0005 for both problems.

For the two moons test problem, GMM, Gaussian linear, and Gaussian linear uniform problems, we train the density estimator for 50 epochs. For SLCP and SLCP distractors, we train the estimator for 200 epochs, and for Bernoulli GLM and Bernoulli GLM raw, we train the estimator for 100 epochs. The number of epochs is chosen based on the complexity of the problem. While we use the default learning rate of 0.0005 for all the problems, for Bernoulli GLM and Bernoulli GLM raw, we found 0.0001 to work better.

5.5 APT

The implementation of Automatic Posterior Transformation, or SNPE-C, is taken from the `sbi` package. As for NPE, we use a pre-configured NSF density estimator from the `sbi` package. The default NSF architecture consists of 5 Piecewise Rational Quadratic Coupling Transforms, each with 50 hidden features and 10 bins. The spline context network includes 1 hidden layer, and the residual network has 2 blocks. The tail bound for each spline is set to 3.0, with no dropout and batch normalization disabled. Since APT is a sequential method, the number of simulations per round is calculated by dividing the simulation budget with the total number of rounds. Similar to NPE we use a `CNNEmbedding` for SIR and LV problems.

5.6 GATSBI

The original paper [Ramesh et al., 2022] provides hyperparameters for two benchmarking problems (two moons and SLCP) from the SBI benchmarking tests. For other test problems, we select and optimize appropriate hyperparameters based on the structure and complexity of each problem. The generator and discriminator layers were selected to reflect the relative complexity, with simpler problems like Gaussian Linear assigned smaller network layers. Specifically, for complex problems like SIR, Lotka-Volterra, SLCP, and SLCP with Distractors, we selected larger network layers to adequately capture their intricacies. For instance, SLCP with Distractors and other high-dimensional problems were assigned generator and discriminator layers similar to SLCP but with additional layers to manage the complexity. The learning rate was consistently set at 0.0001, balancing convergence speed and stability. Noise injection layers were tailored to each problem to ensure sufficient variability in the generated data, enhancing robustness. As recommended in the original article, the batch size is defined as the smaller value between 10% of the simulation budget and 1000. Each epoch comprised 10 discriminator updates and 10 generator updates. For each simulation budget, 100 samples are used for validation. We used the Adam optimizer with a learning rate of 0.0001, $\beta_1 = 0.9$, and $\beta_2 = 0.99$. Noise injection details are provided in the table. Each discriminator has a single output feature in the last layer, followed by a sigmoid nonlinearity. Each layer (except the last) is followed by a leaky ReLU nonlinearity with a slope of 0.1. Note: We only consider the amortized GATSBI here and do not test on sequential GATSBI, which, as stated in the original paper, is computationally very expensive.

Table 4: GATSBI hyperparameters.

Problem	Generator Layers	Discriminator Layers	Noise Layer
Gaussian Linear	(64, 64, 64, 64, 10)	(1024, 1024, 1024, 1)	2
Gaussian Linear Uniform	(64, 64, 64, 64, 10)	(1024, 1024, 1024, 1)	2
SLCP	(128, 128, 128, 128, 5)	(2048, 2048, 2048, 2048, 2048, 1)	4
SLCP with Distractors	(128, 128, 128, 128, 5)	(2048, 2048, 2048, 2048, 2048, 1)	4
Bernoulli GLM	(128, 128, 128, 128, 10)	(2048, 2048, 2048, 1)	2
Bernoulli GLM Raw	(128, 128, 128, 128, 10)	(2048, 2048, 2048, 1)	2
Gaussian Mixture	(64, 2)	(1024, 1024, 1024, 1)	2
Two Moons	(128, 2)	(2048, 2048, 2048, 1)	2
SIR	(128, 128, 128, 128, 2)	(2048, 2048, 2048, 2048, 2048, 1)	4
Lotka-Volterra	(128, 128, 128, 128, 4)	(2048, 2048, 2048, 2048, 2048, 1)	4

6 Training Times

We present the training times involved for various methods across different simulation budgets for each test problem in Table 5. We observe that variational methods result in faster training times compared to other approaches, except the Gaussian Linear and Gaussian Linear Uniform test problems where JANA is the fastest to train. However, as will be shown in subsequent sections, flow-based approaches generally approximate the posterior distribution more accurately. The methods are built on distinct generative modeling frameworks, which inherently affect their training times; for instance, APT requires multiple rounds of inference, while GAN-based models, as noted in the original paper, were trained over several iterations. These comparisons presented herein are general estimates primarily indicating efficiency, highlighting the trade-off between training speed and posterior inference quality. The experiments were conducted using, and are subject to the hyperparameter settings described in Section 5.

Table 5: Training time for different methods across simulation budgets (mean \pm std. dev.) in minutes.

(a) SLCP Distractors, Bernoulli GLM Raw, Lotka Volterra.

Method	SLCP Distractors			Bernoulli GLM Raw			Lotka Volterra		
Budget	10,000	20,000	30,000	10,000	20,000	30,000	10,000	20,000	30,000
GATSBI	74.3781 (\pm 2.5913)	100.5944 (\pm 2.3908)	102.3091 (\pm 0.5192)	114.7599 (\pm 1.1907)	115.2224 (\pm 1.4337)	144.1059 (\pm 24.1544)	78.9107 (\pm 6.3269)	75.7348 (\pm 0.7060)	74.9980 (\pm 0.2068)
NPE	21.9236 (\pm 2.4140)	43.9272 (\pm 2.5815)	64.3851 (\pm 7.1397)	25.3937 (\pm 2.0968)	61.4381 (\pm 2.6192)	85.9497 (\pm 6.5533)	80.6703 (\pm 14.6147)	160.9298 (\pm 42.8261)	188.0471 (\pm 29.4658)
JANA	8.4922 (\pm 0.0697)	13.5946 (\pm 0.2462)	20.5680 (\pm 0.1282)	24.0211 (\pm 0.3794)	44.2124 (\pm 0.2311)	64.5062 (\pm 1.0102)	7.5911 (\pm 0.0260)	13.2857 (\pm 0.1478)	18.5595 (\pm 0.0819)
APT	26.3062 (\pm 0.3652)	49.9643 (\pm 2.7334)	74.3185 (\pm 2.5450)	21.8751 (\pm 1.2827)	40.0059 (\pm 1.3773)	60.9409 (\pm 3.0002)	45.5259 (\pm 4.8561)	96.1541 (\pm 13.7757)	144.3338 (\pm 18.3333)
CP-VAE	1.5425 (\pm 0.3400)	3.6225 (\pm 0.7671)	4.6336 (\pm 1.5291)	6.0440 (\pm 0.9923)	14.5025 (\pm 0.1864)	10.3627 (\pm 0.2098)	7.2281 (\pm 3.2522)	14.6196 (\pm 1.9244)	22.8725 (\pm 1.8407)
UP-VAE	1.8949 (\pm 0.1575)	2.8521 (\pm 0.3998)	4.2508 (\pm 0.5292)	3.4259 (\pm 0.4947)	8.6454 (\pm 2.8058)	14.2115 (\pm 7.2751)	2.8963 (\pm 0.5278)	4.9398 (\pm 0.1074)	7.1680 (\pm 1.2662)

(b) Gaussian Mixture, Gaussian Linear, Gaussian Linear Uniform, SLCP.

Method	Gaussian Mixture			Gaussian Linear			Gaussian Linear Uniform			SLCP		
Budget	10,000	20,000	30,000	10,000	20,000	30,000	10,000	20,000	30,000	10,000	20,000	30,000
GATSBI	114.0701 (\pm 2.1061)	111.3030 (\pm 0.2751)	137.4563 (\pm 19.1572)	48.1855 (\pm 0.2364)	48.6964 (\pm 0.8421)	49.1194 (\pm 0.4861)	43.2740 (\pm 0.3636)	66.4335 (\pm 5.7030)	69.1033 (\pm 0.1487)	162.7208 (\pm 14.7302)	196.1914 (\pm 119.4162)	99.3880 (\pm 5.6326)
NPE	19.5554 (\pm 2.4731)	42.8758 (\pm 4.5424)	64.0252 (\pm 6.5075)	12.0300 (\pm 0.8048)	24.6934 (\pm 1.6287)	38.7897 (\pm 1.2305)	16.5508 (\pm 0.8518)	30.9049 (\pm 2.7695)	49.4179 (\pm 1.4930)	42.9682 (\pm 6.3522)	97.7035 (\pm 6.6633)	117.6113 (\pm 4.1221)
JANA	7.1898 (\pm 0.0272)	13.9497 (\pm 0.9445)	17.1399 (\pm 0.1039)	2.2083 (\pm 0.02908)	3.6762 (\pm 0.0545)	5.2089 (\pm 0.05405)	1.8213 (\pm 0.0194)	2.9596 (\pm 0.0081)	4.0954 (\pm 0.0271)	29.3388 (\pm 0.6019)	53.7567 (\pm 1.0519)	76.1879 (\pm 5.7094)
APT	76.2690 (\pm 7.0242)	167.8838 (\pm 15.9919)	240.1324 (\pm 22.7401)	70.4689 (\pm 0.8763)	135.3840 (\pm 5.7490)	203.2690 (\pm 5.9727)	78.6141 (\pm 2.1101)	158.5665 (\pm 9.3247)	219.4443 (\pm 11.8299)	93.4032 (\pm 1.2551)	150.2933 (\pm 11.1011)	216.3000 (\pm 21.3758)
CP-VAE	2.3730 (\pm 0.8103)	4.6713 (\pm 1.1037)	5.1945 (\pm 0.9081)	3.113960 (\pm 0.579760)	5.2455 (\pm 0.6261)	6.4933 (\pm 1.3784)	3.3643 (\pm 0.5935)	7.4822 (\pm 1.6540)	8.4451 (\pm 2.4702)	3.8463 (\pm 0.6165)	11.3799 (\pm 1.9730)	19.5251 (\pm 2.9897)
UP-VAE	5.6148 (\pm 1.2006)	6.2974 (\pm 1.2917)	12.9608 (\pm 1.4142)	5.7494 (\pm 1.1620)	9.1472 (\pm 1.0260)	9.1583 (\pm 1.7428)	7.4118 (\pm 1.8465)	14.0751 (\pm 1.5503)	18.6407 (\pm 6.5659)	5.4909 (\pm 0.6476)	12.5897 (\pm 1.1725)	22.6865 (\pm 3.2339)

7 Additional results

We present herein the approximated posterior distributions for all test problems, corresponding to a maximum simulation budget of 30,000.

7.1 Two Moons

The challenge lies not only in accurately recovering the bimodal posterior distribution but also in capturing the distinct crescent shape inherent in the data.

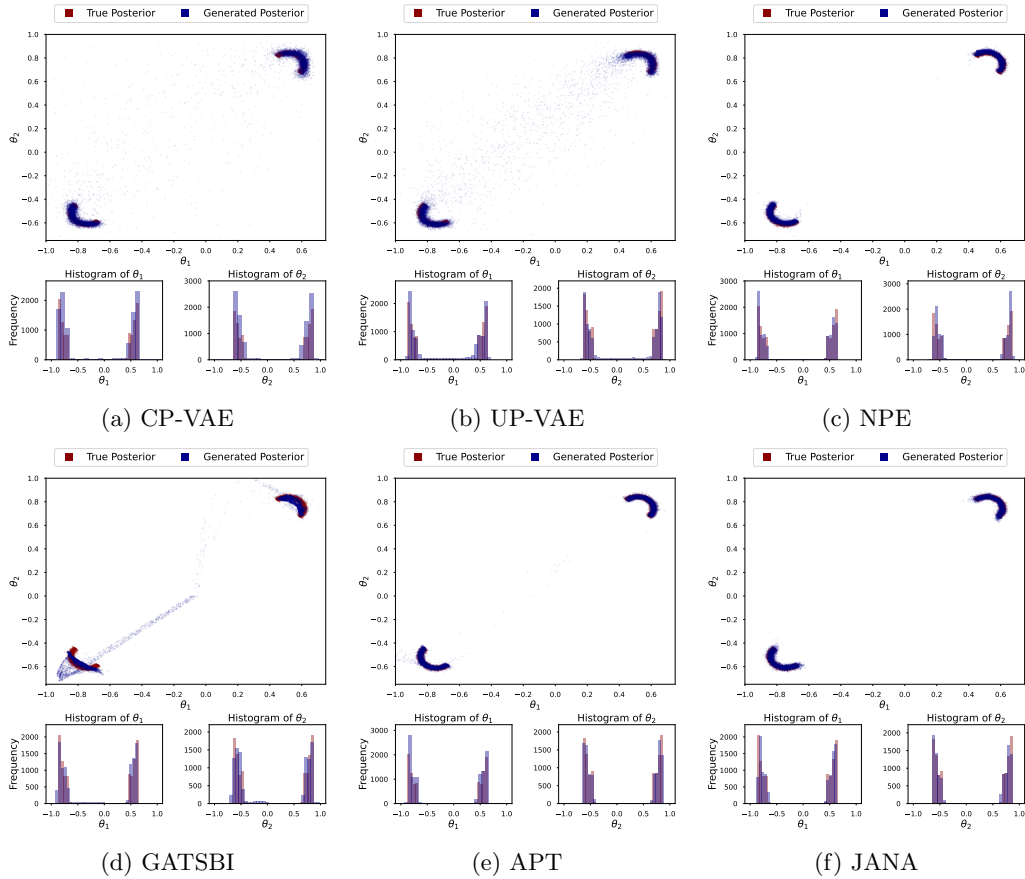
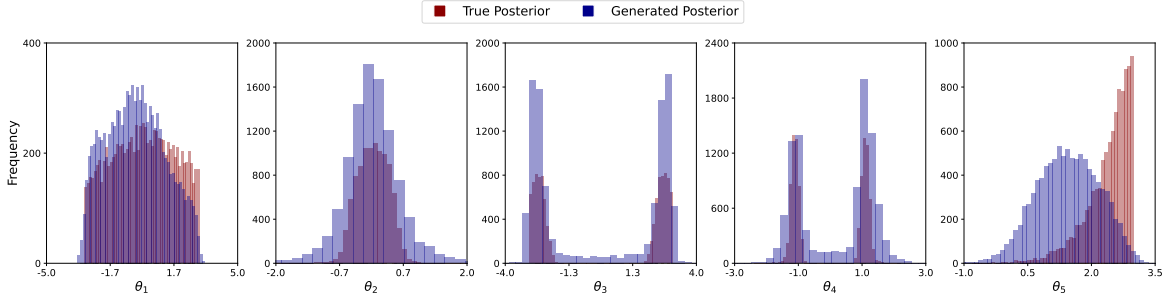


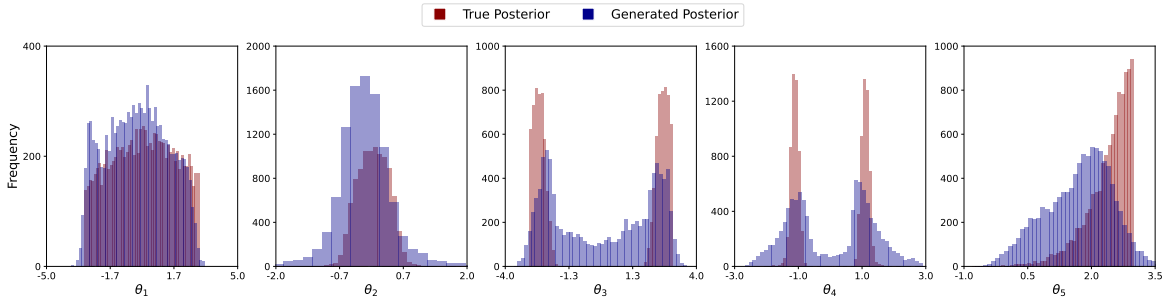
Figure 1: Comparison of the estimated posterior distributions for the Two Moons test problem (simulation budget: 30,000).

7.2 SLCP

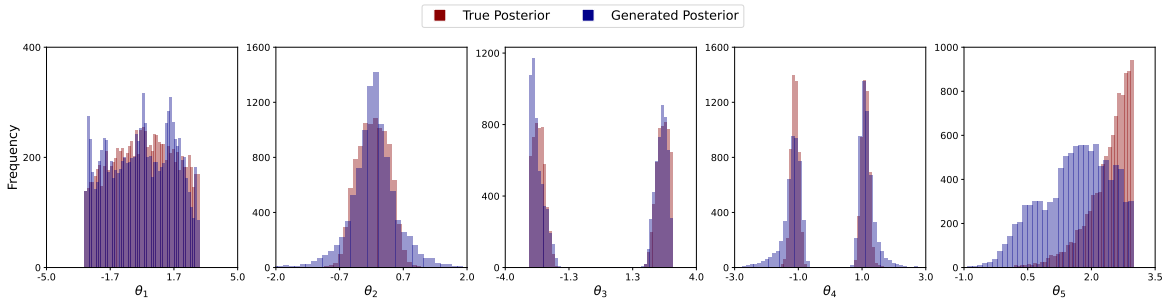
The posterior distribution corresponding to this model exhibits a diverse range of behaviors across the parameters. Specifically, θ_1 resembles a uniform distribution, θ_2 follows an approximately Gaussian distribution, while θ_3 and θ_4 are highly multimodal. Additionally, θ_5 displays a skewed, unimodal distribution. These complex characteristics make the posterior challenging to approximate accurately.



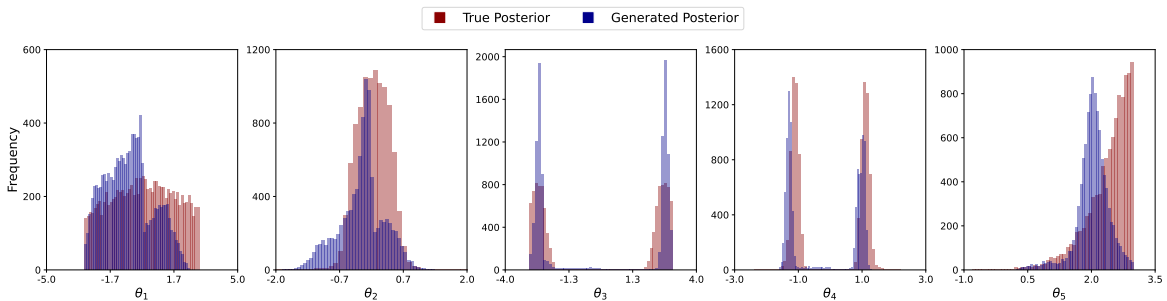
(a) CP-VAE



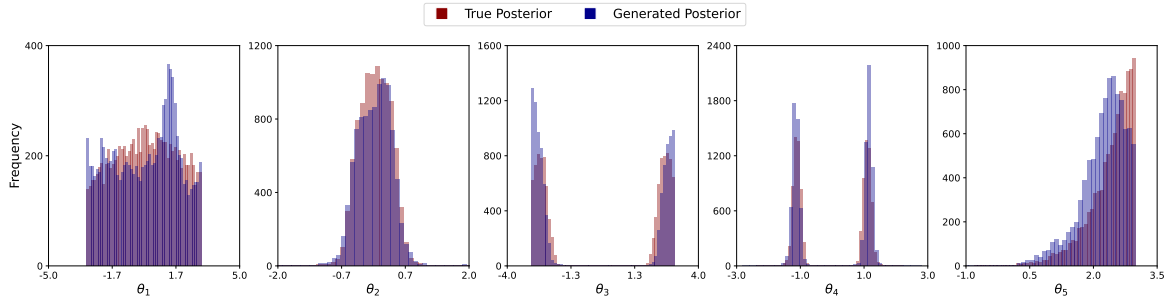
(b) UP-VAE



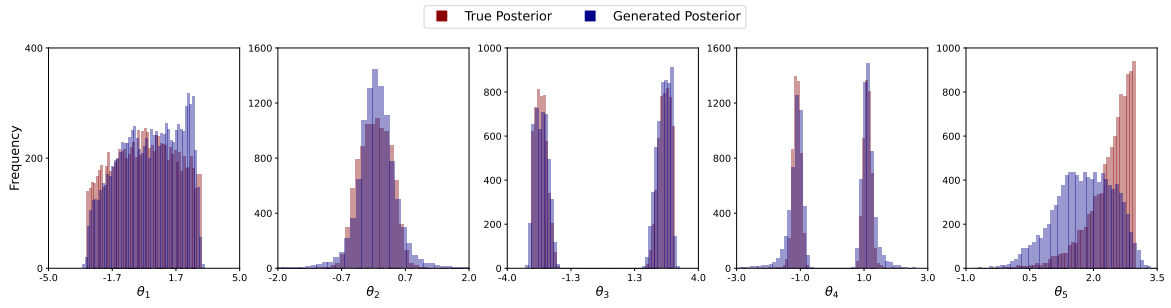
(c) NPE



(d) GATSBI



(a) APT



(b) JANA

Figure 3: Comparison of estimated posterior distributions for the SLCP test problem (simulation budget: 30,000).

7.3 Gaussian Mixture

In this test problem, the challenge lies in identifying the shared mean of two distinct Gaussian distributions. These distributions differ in their variance scales, with one exhibiting a significantly broader covariance than the other, making it essential to effectively model their interaction to achieve accurate posterior inference.

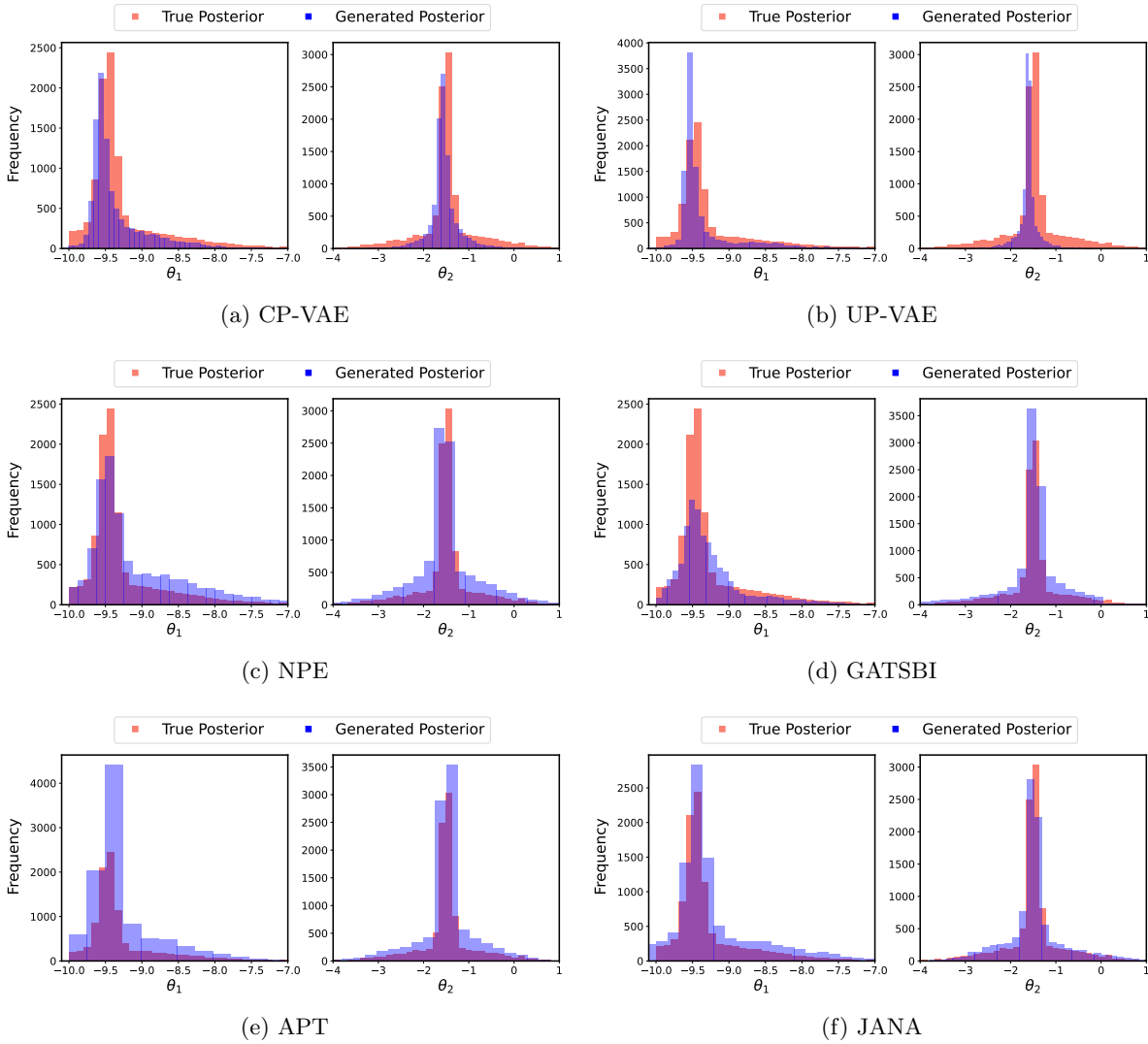
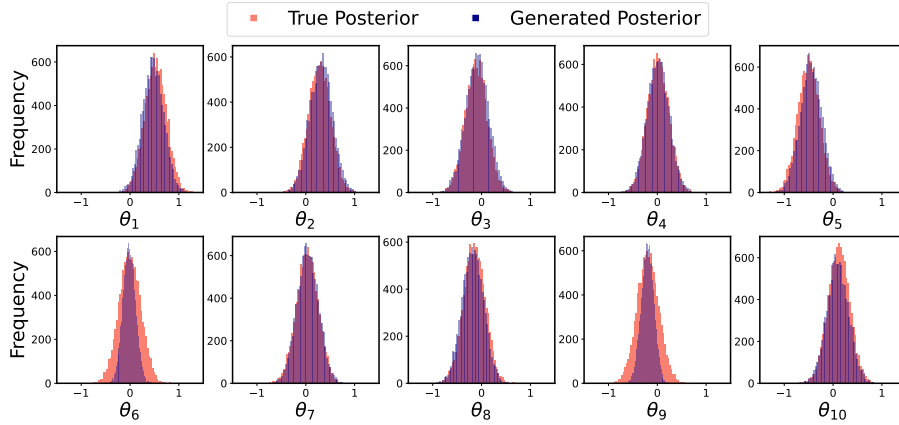


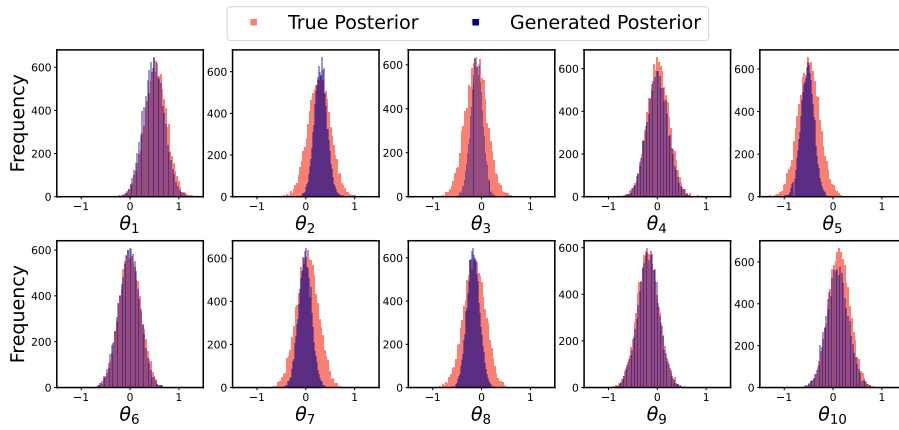
Figure 4: Comparison of estimated posterior distributions for the Gaussian Mixture Model test problem (simulation budget: 30,000).

7.4 Gaussian Linear

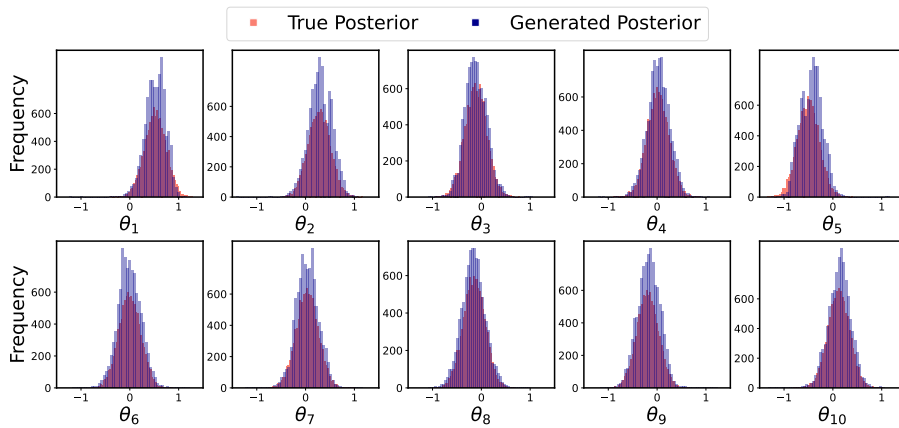
In this test problem, both the prior and likelihood are Gaussian, resulting in a conjugate prior that ensures that the posterior is also Gaussian. The primary challenge lies in accurately inferring the posterior mean θ , which tests the efficacy of SBI methods in capturing the true underlying distribution.



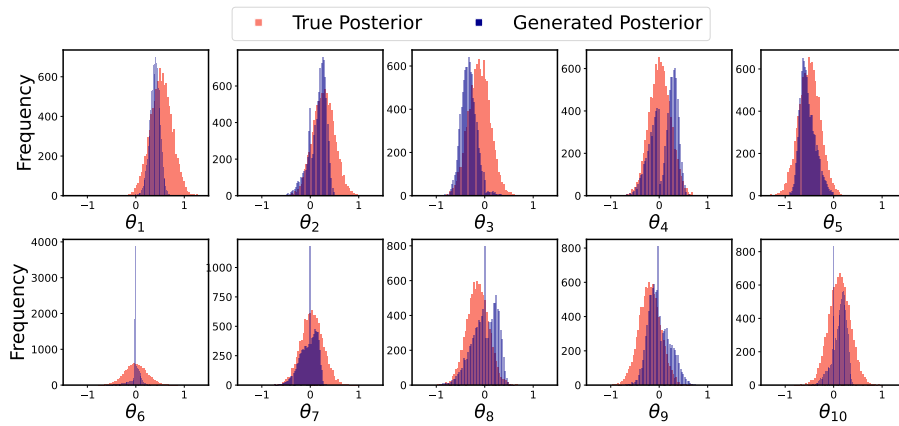
(a) CP-VAE



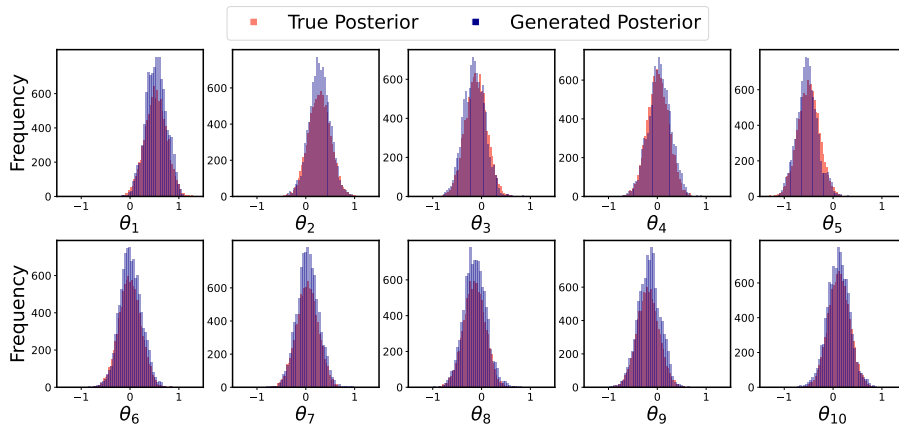
(b) UP-VAE



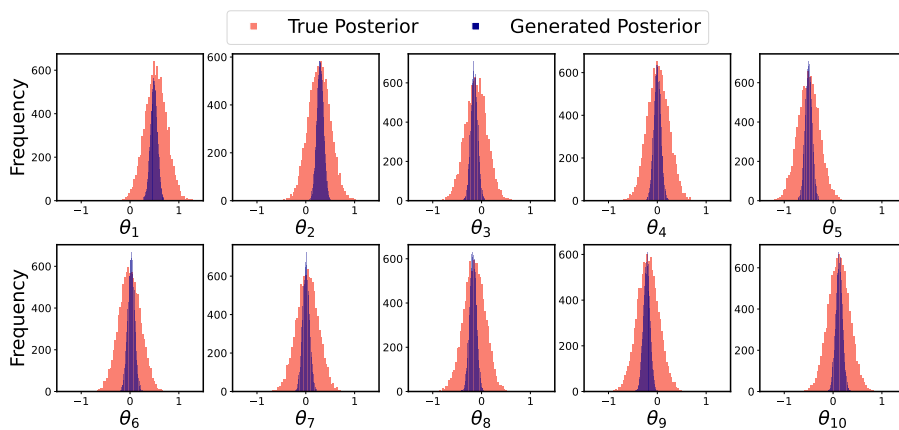
(c) NPE



(a) GATSBI



(b) APT

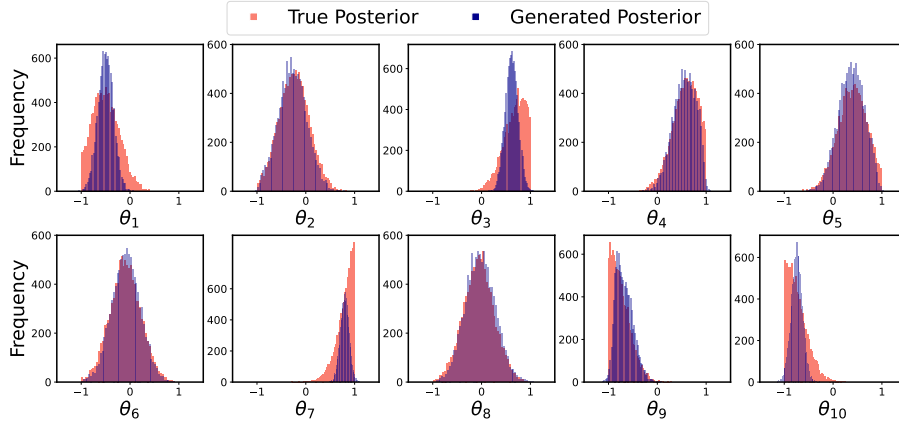


(c) JANA

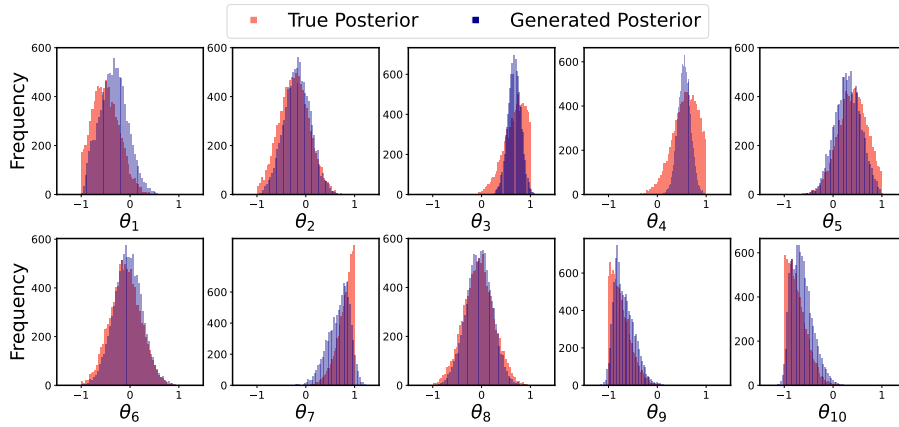
Figure 6: Comparison of estimated posterior distributions for the Gaussian Linear Model test problem (simulation budget: 30,000).

7.5 Gaussian Linear Uniform

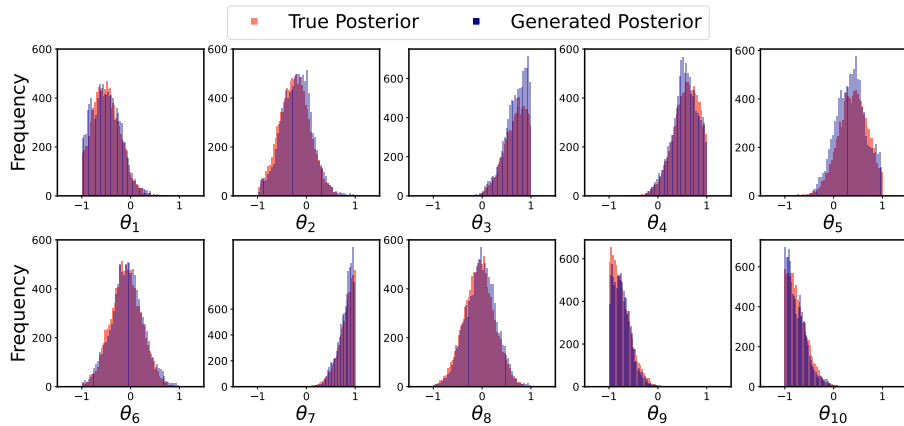
The Gaussian Linear Uniform model utilizes a uniform prior, representing a non-informative approach in contrast to the Gaussian prior used in the standard Gaussian Linear model. This non-conjugate setting complicates the integration of the Gaussian likelihood with the uniform prior, potentially resulting in a more intricate posterior distribution. As a result, effectively inferring the parameter θ tests the robustness of SBI methods in handling uncertainty and variability inherent in the data.



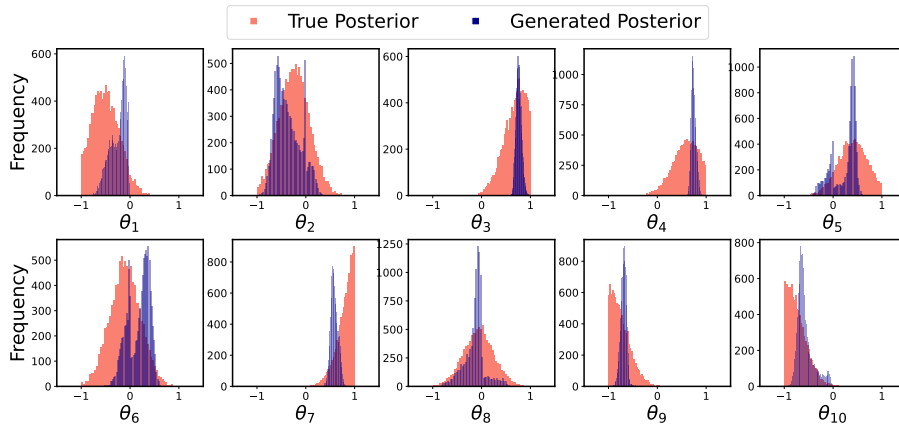
(a) CP-VAE



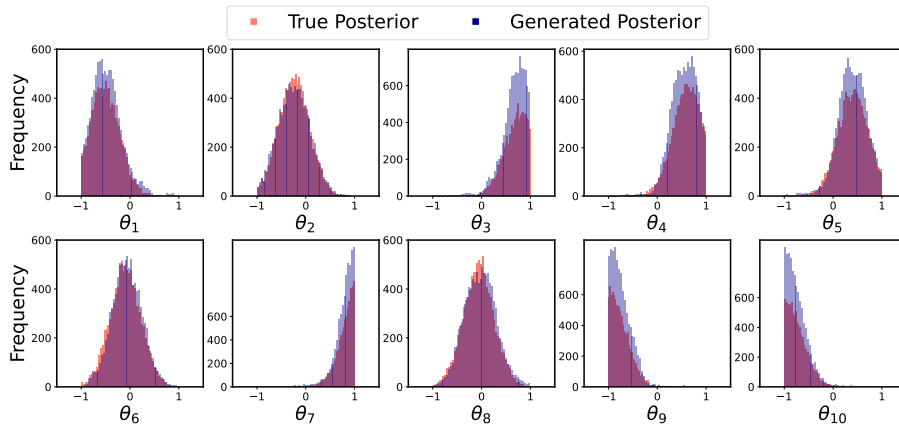
(b) UP-VAE



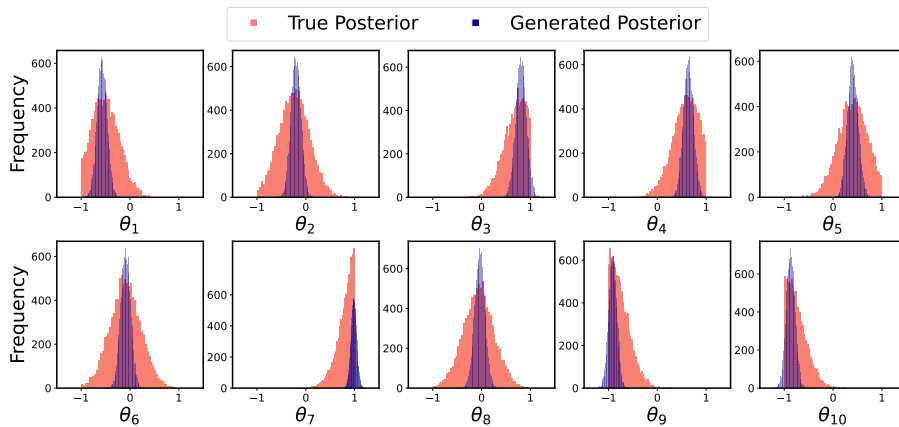
(c) NPE



(a) GATSBI



(b) APT

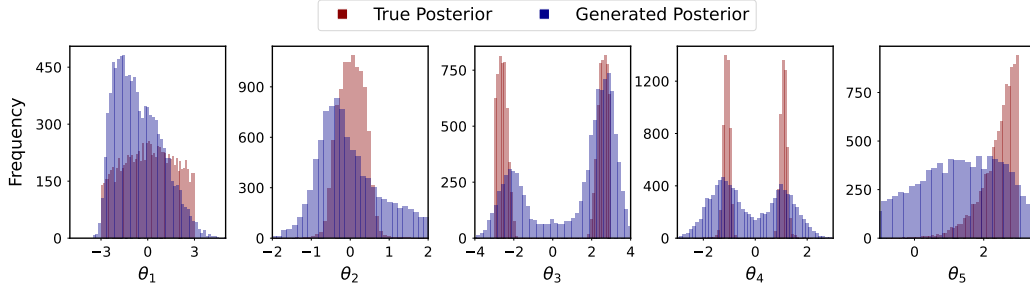


(c) JANA

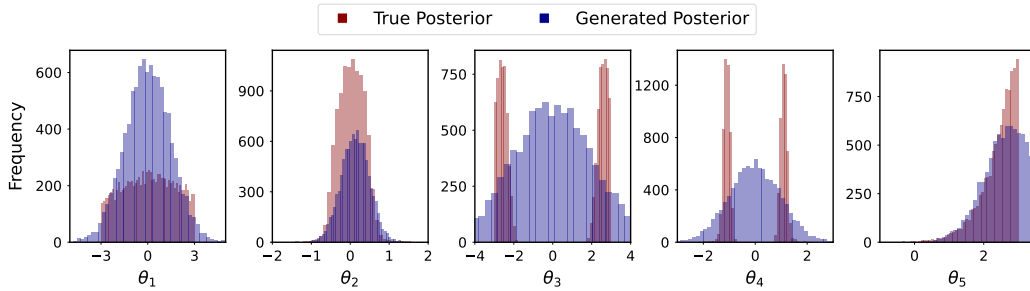
Figure 8: Comparison of estimated posterior distributions for the Gaussian Linear Uniform test problem (simulation budget: 30,000).

7.6 SLCP with distractors

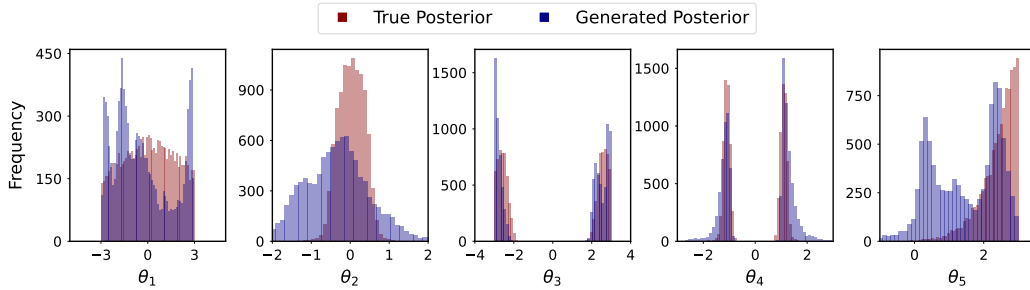
This task extends the SLCP test problem by incorporating uninformative dimensions, or distractors, into the observations. The challenge lies in effectively inferring the posterior distributions while navigating the increased dimensionality and noise introduced by these irrelevant features.



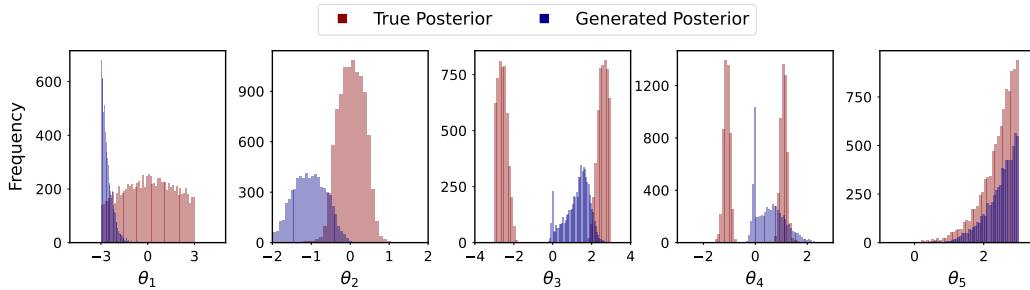
(a) CP-VAE



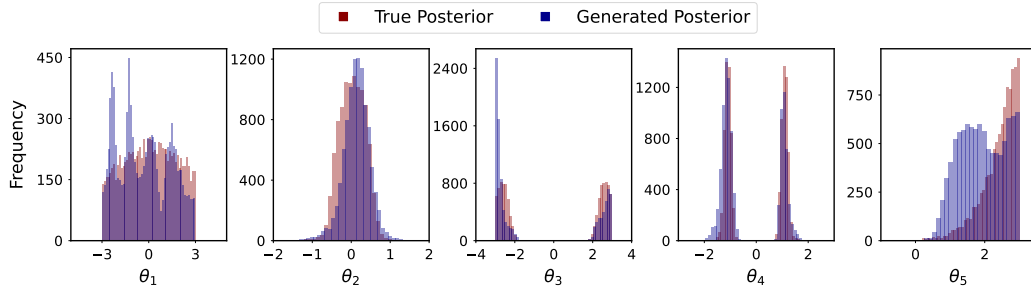
(b) UP-VAE



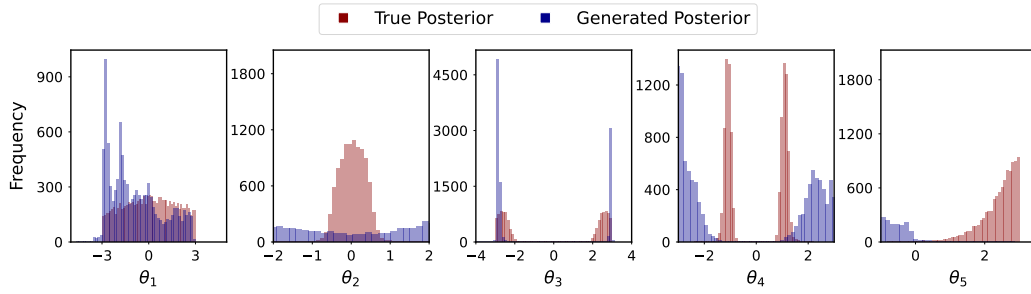
(c) NPE



(d) GATSBI



(a) APT

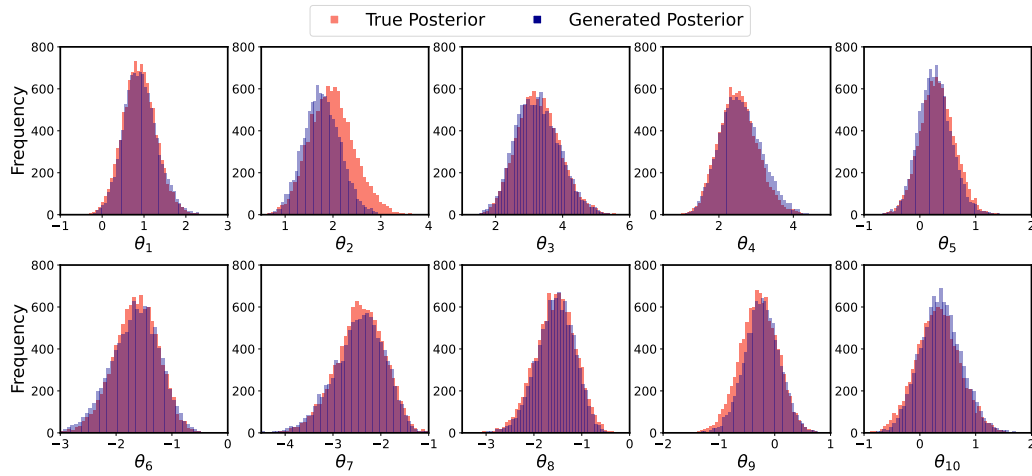


(b) JANA

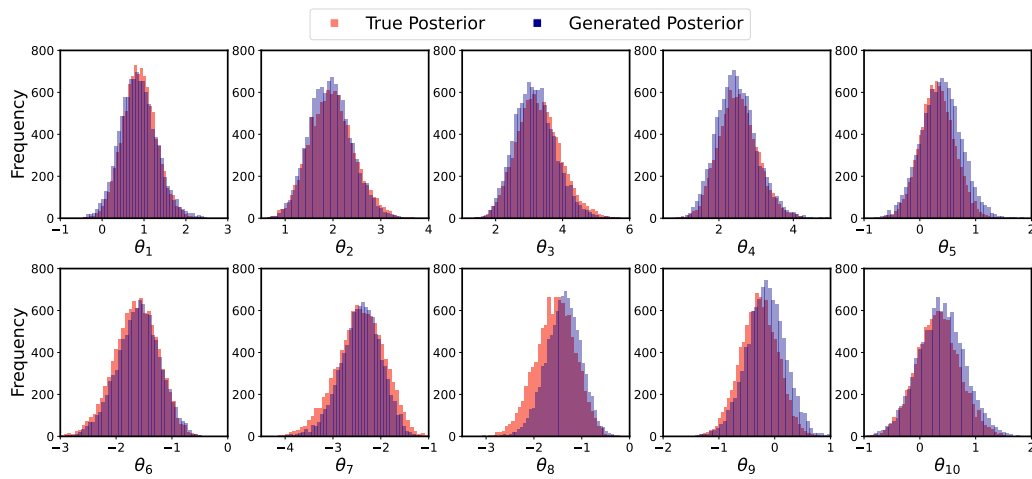
Figure 10: Comparison of estimated posterior distributions for the SLCP test problem with distractors (simulation budget: 30,000).

7.7 Bernoulli GLM Model

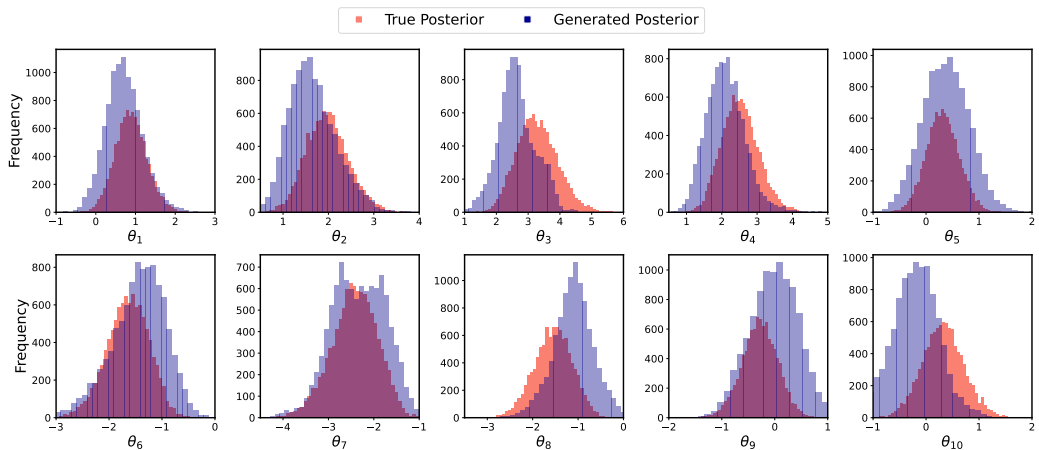
This model tests the effectiveness of SBI methods in estimating the posterior distribution of a 10-parameter generalized linear model with Bernoulli observations and a Gaussian prior.



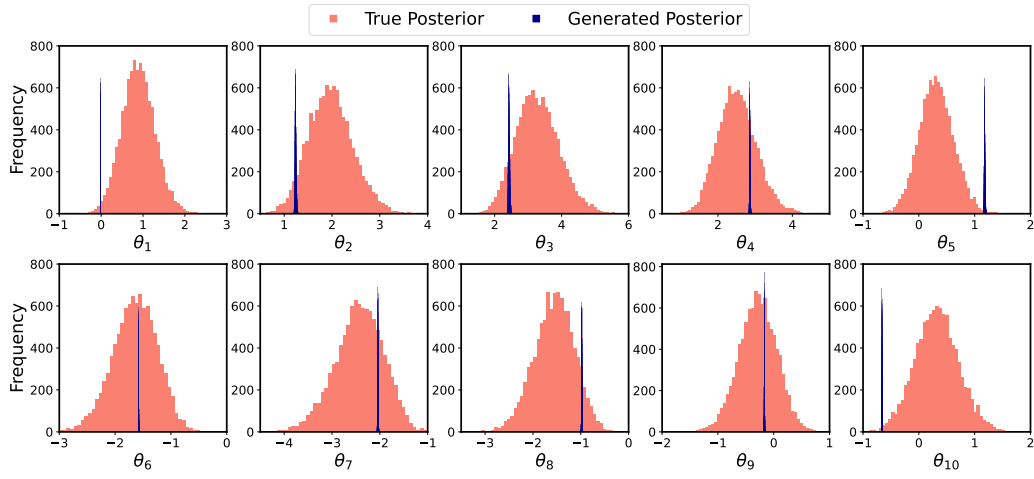
(a) CP-VAE



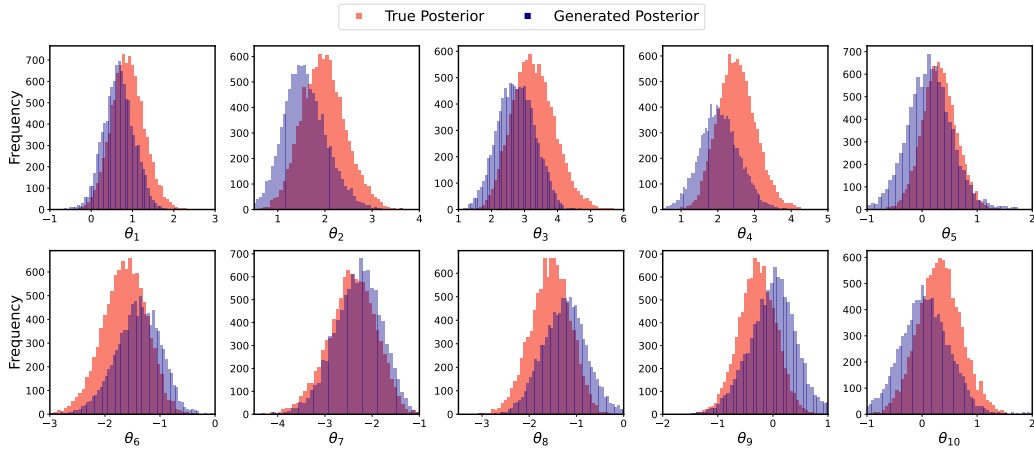
(b) UP-VAE



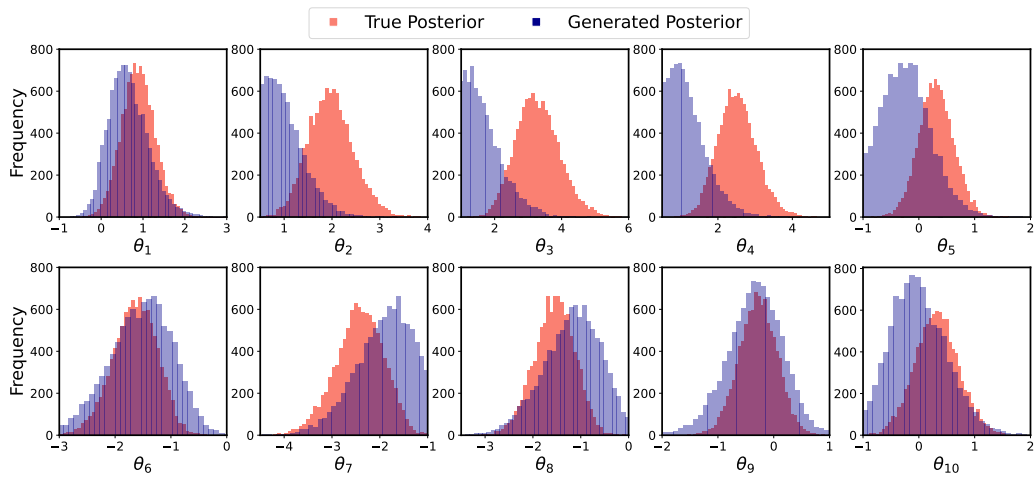
(c) NPE



(a) GATSBI



(b) APT

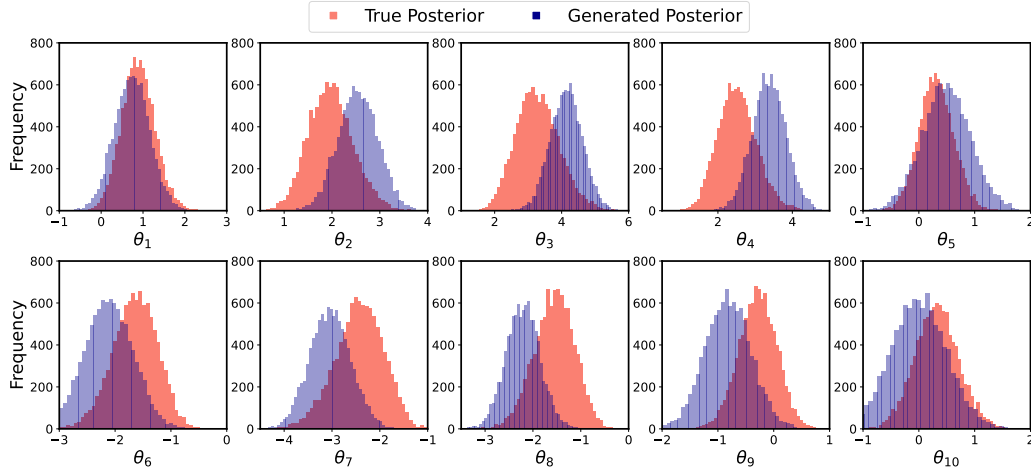


(c) JANA

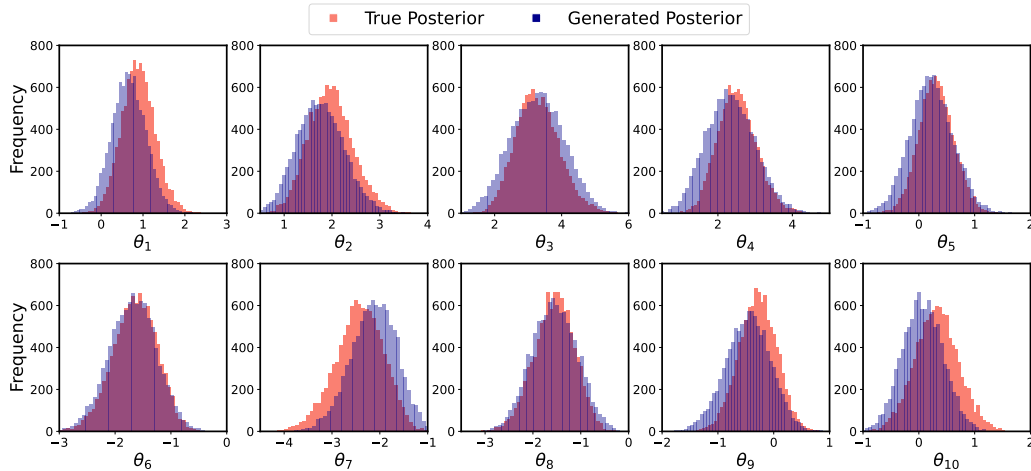
Figure 12: Comparison of estimated posterior distributions for the Bernoulli GLM test problem (simulation budget: 30,000).

7.8 Bernoulli GLM Raw

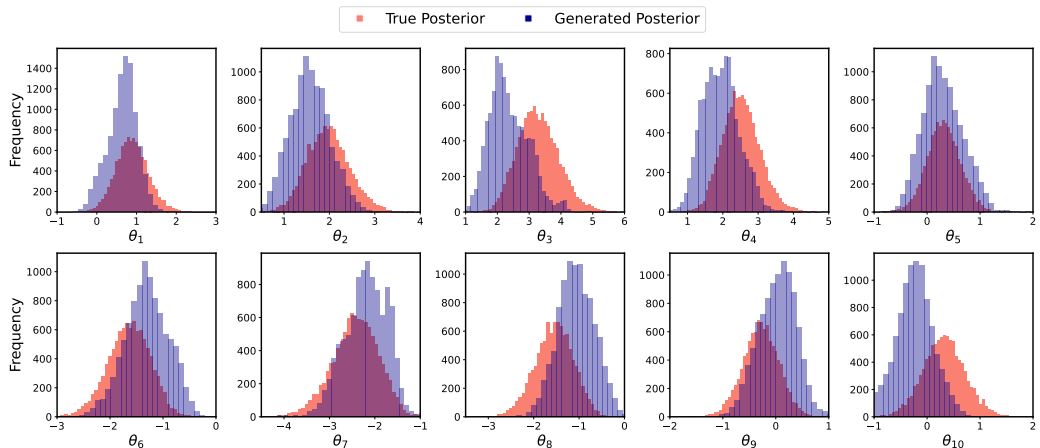
This task is an extension of Bernoulli Generalized Linear Model (GLM) where raw observations are used instead of sufficient statistics. This alteration introduces additional complexity, as the raw data must be effectively managed to infer the underlying parameters.



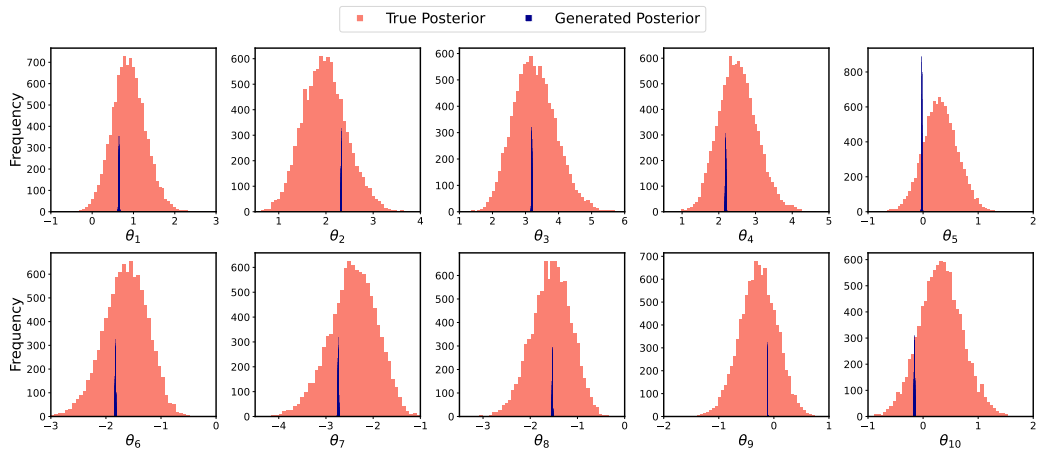
(a) CP-VAE



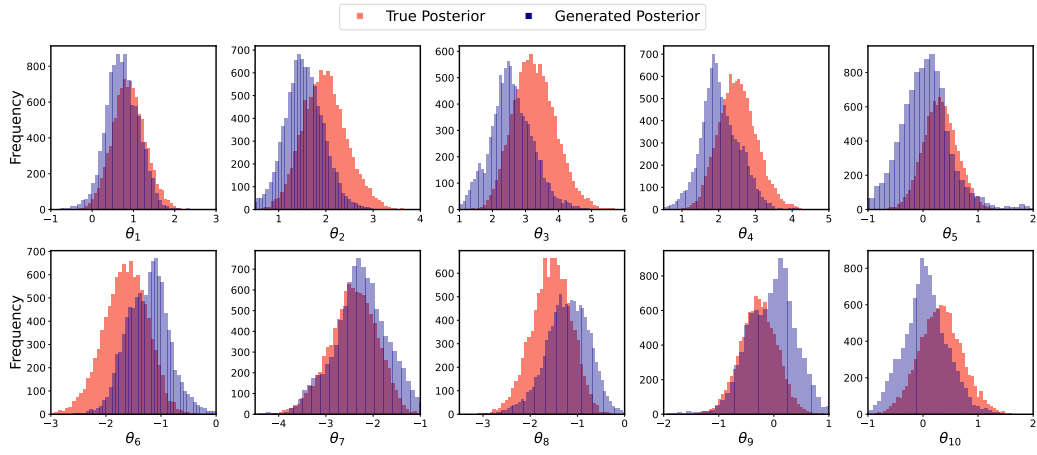
(b) UP-VAE



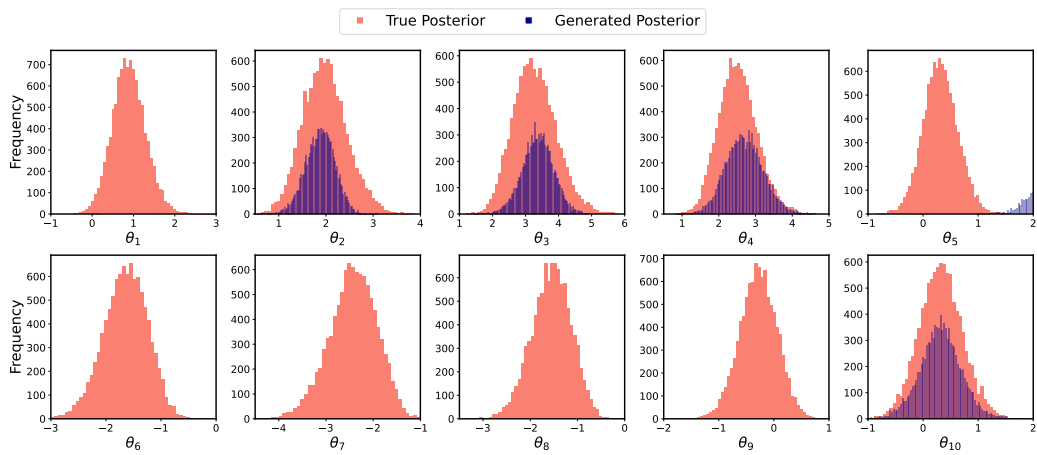
(c) NPE



(a) GATSBI



(b) APT

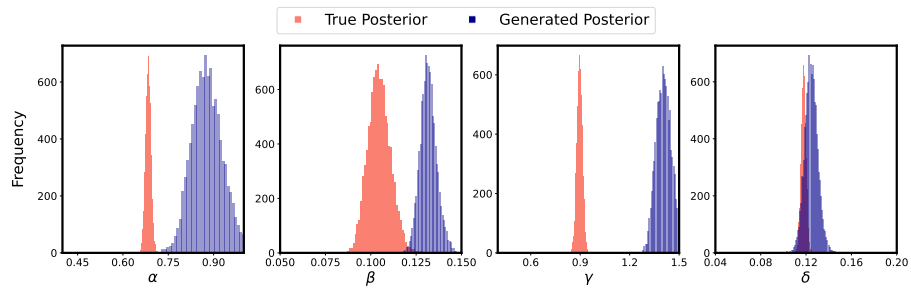


(c) JANA

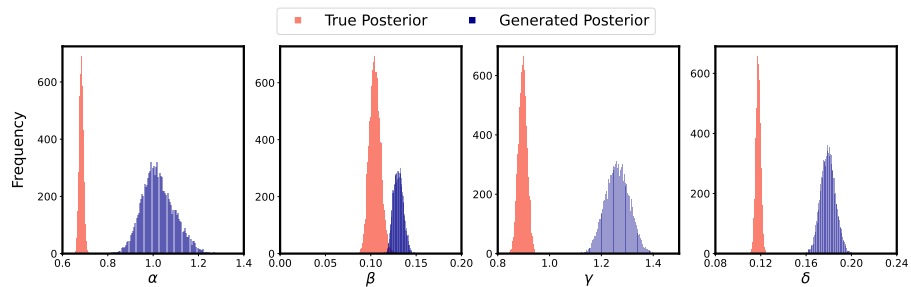
Figure 14: Comparison of estimated posterior distributions for the Bernoulli GLM Raw test problem (simulation budget: 30,000).

7.9 Lotka Volterra

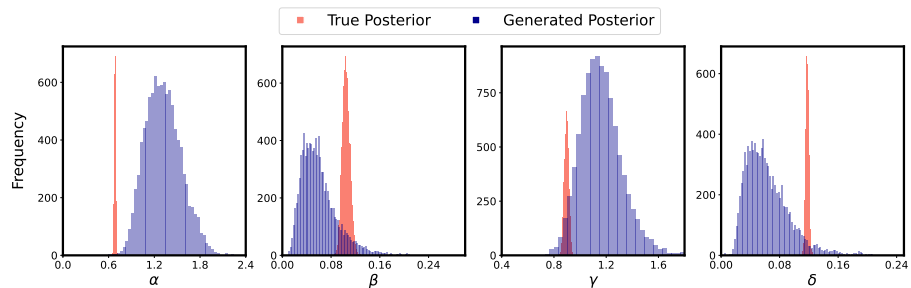
The Lotka-Volterra model comprises a challenging test problem for posterior inference due to its non-linear dynamics and potential chaotic behavior in predator-prey interactions. Accurately estimating the underlying parameters from observed ecological time-series data requires robust SBI methods to navigate the model's stiffness and complexity.



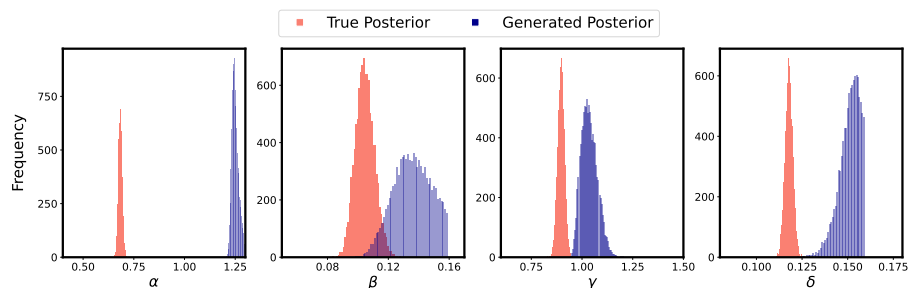
(a) CP-VAE



(b) UP-VAE



(c) NPE



(d) GATSBI

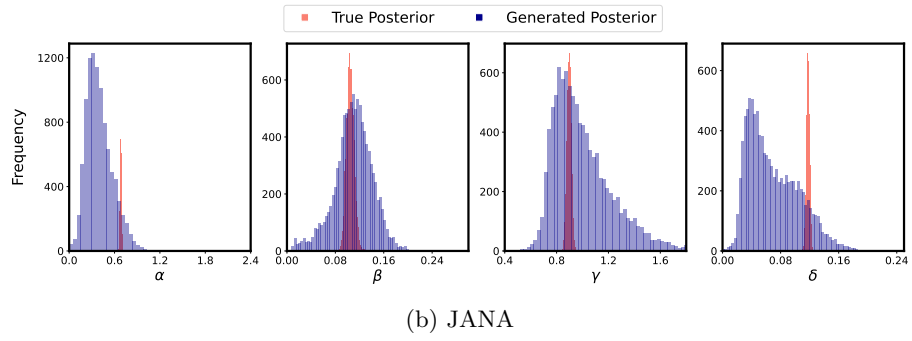
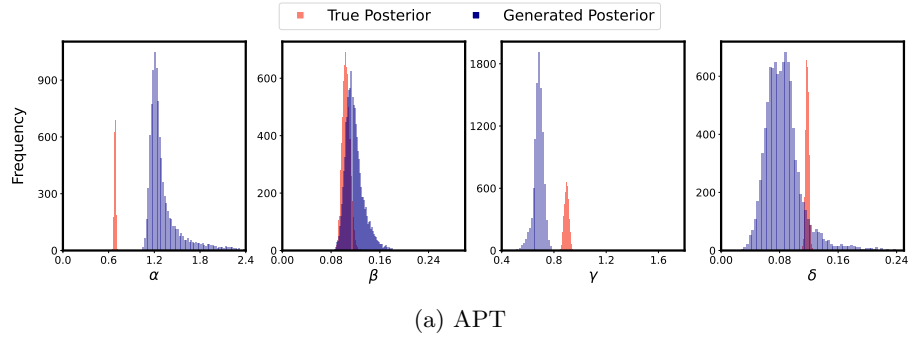


Figure 16: Comparison of estimated posterior distributions for the Lotka Volterra test problem (simulation budget: 30,000).

7.10 SIR

In the SIR model, the task is to infer the posterior distributions of the contact and recovery rates based on the sampled number of infectious individuals at 10 evenly spaced time points. This requires robust simulation-based inference methods to address the challenges posed by highly variable and noisy infection data.

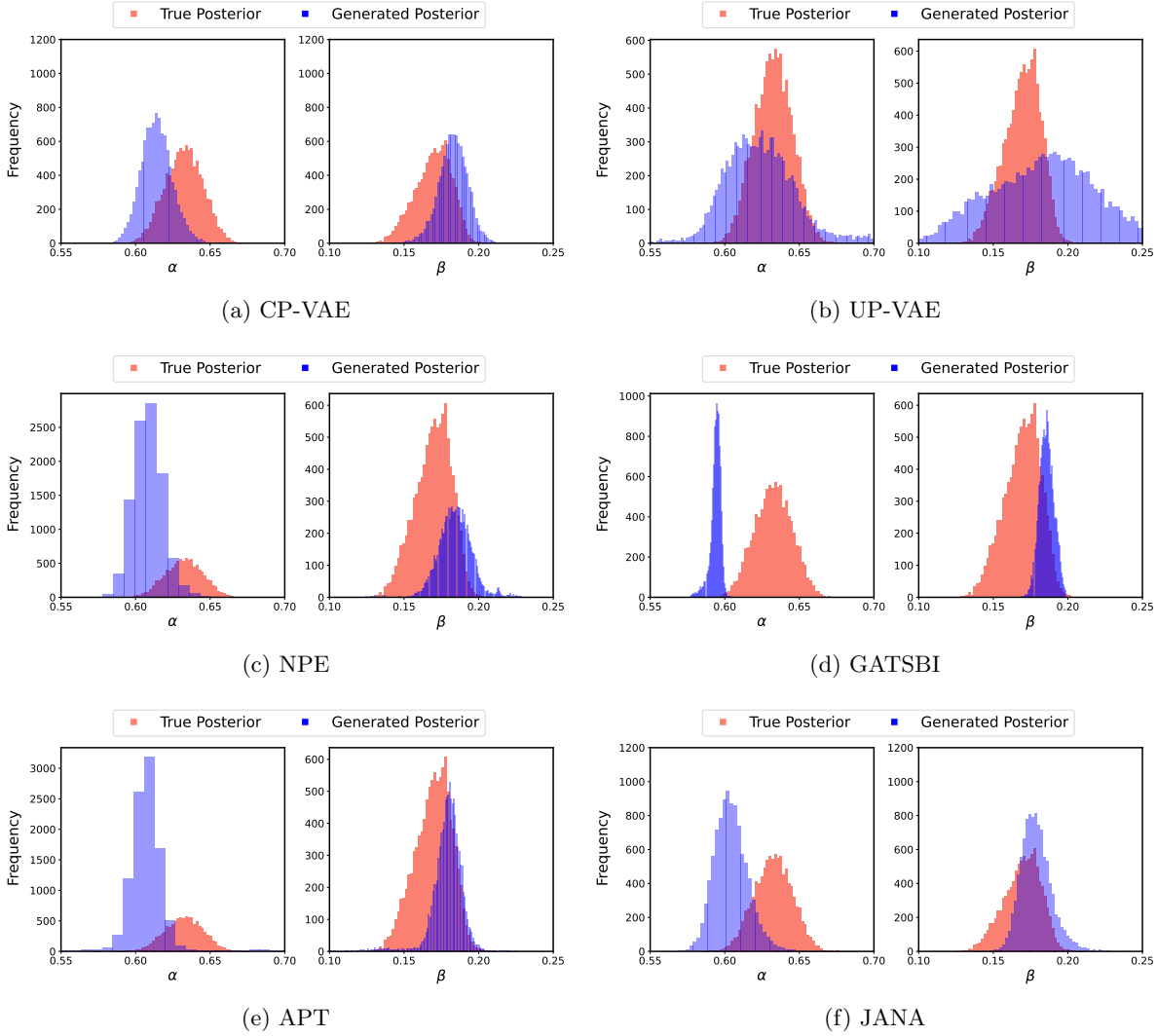


Figure 17: Comparison of estimated posterior distributions for the SIR test problem (simulation budget: 30,000).

8 SBI Metrics

In this section, we introduce the metrics used to evaluate SBI methods. We discuss how these metrics are calculated and highlight some of their potential drawbacks.

8.1 C2ST

The Classifier Two-Sample Test (C2ST) is a statistical method used to compare two probability distributions by training a classifier to differentiate between samples from each distribution [Friedman, 2003]. This method is particularly useful in SBI for assessing the similarity between a generated posterior distribution and the true posterior distribution. The process of the Classifier Two-Sample Test (C2ST) involves combining samples from two distributions, P (e.g., simulated posterior) and Q (e.g., true posterior), into a single dataset, labeling the

samples from P and Q as distinct classes, and training a binary classifier such as a neural network or logistic regression on this labeled dataset. The classifier’s accuracy on a test set indicates the similarity between the distributions: a C2ST metric of 0.5 signifies no distinguishable difference, while a value higher than 0.5 suggests significant differences. To estimate the C2ST metric, we use the method described in the [Lueckmann et al., 2021], where a two-layer neural network with ReLU non-linearity, and ten times as many units as the dimensionality of the parameters is trained. This training involves 10,000 z-score normalized samples from both the reference and approximate posteriors, with classification accuracy reported via 5-fold cross-validation. While the C2ST metric is a powerful tool for validating simulation models, it is sensitive and can be challenging to interpret; for example, the score may reach 1 even if one dimension is poorly estimated, regardless of the accuracy in other dimensions. Additionally, the metric’s outcome depends on the classifier parameters, necessitating careful methodological consideration.

Table 6: C2ST metric for different methods across simulation budgets (mean \pm std. dev.).

(a) SLCP Distractors, Bernoulli GLM Raw, Lotka Volterra.

Method	SLCP Distractors			Bernoulli GLM Raw			Lotka Volterra			
	Budget	10,000	20,000	30,000	10,000	20,000	30,000	10,000	20,000	30,000
GATSBI	0.9995 (\pm 0.0007)	0.9978 (\pm 0.0016)	0.9994 (\pm 0.0004)	0.9998 (\pm 0.0001)	0.9999 (\pm 0.0001)	0.9999 (\pm 0.0000)	0.9999 (\pm 0.0001)	0.9999 (\pm 0.0000)	0.9999 (\pm 0.0000)	1.0 (\pm 0.0000)
NPE	0.9714 (\pm 0.0144)	0.9468 (\pm 0.0157)	0.9359 (\pm 0.0127)	0.9354 (\pm 0.0093)	0.9114 (\pm 0.0082)	0.9065 (\pm 0.0105)	0.9999 (\pm 0.0001)	0.9999 (\pm 0.0000)	0.9999 (\pm 0.0000)	0.9999 (\pm 0.0000)
JANA	0.9987 (\pm 0.0010)	0.9945 (\pm 0.0138)	0.9933 (\pm 0.0654)	0.9997 (\pm 0.0007)	1.0 (\pm 0.0000)	1.0 (\pm 0.0000)	0.9999 (\pm 0.0000)	0.9998 (\pm 0.0001)	0.9998 (\pm 0.0001)	0.9998 (\pm 0.0001)
APT	0.9823 (\pm 0.0055)	0.9451 (\pm 0.0158)	0.9130 (\pm 0.0301)	0.8455 (\pm 0.0116)	0.8596 (\pm 0.0152)	0.8461 (\pm 0.0135)	0.9999 (\pm 0.0001)	0.9999 (\pm 0.0000)	0.9999 (\pm 0.0001)	0.9999 (\pm 0.0001)
CP-VAE	0.9956 (\pm 0.0037)	0.9880 (\pm 0.0057)	0.9746 (\pm 0.0075)	0.9491 (\pm 0.0078)	0.9171 (\pm 0.0258)	0.9307 (\pm 0.0000)	0.9999 (\pm 0.0001)	0.9999 (\pm 0.0001)	0.9999 (\pm 0.0001)	0.9999 (\pm 0.0001)
UP-VAE	0.9838 (\pm 0.0036)	0.9798 (\pm 0.0023)	0.9840 (\pm 0.0053)	0.8674 (\pm 0.0493)	0.8790 (\pm 0.0363)	0.8536 (\pm 0.0460)	0.9999 (\pm 0.0001)	0.9999 (\pm 0.0001)	0.9999 (\pm 0.0001)	0.9999 (\pm 0.0001)

(b) Gaussian Mixture, Gaussian Linear, Gaussian Linear Uniform, SLCP.

Method	Gaussian Mixture			Gaussian Linear			Gaussian Linear Uniform			SLCP		
	Budget	10,000	20,000	30,000	10,000	20,000	30,000	10,000	20,000	30,000	10,000	20,000
GATSBI	0.7474 (\pm 0.0364)	0.6977 (\pm 0.0260)	0.7234 (\pm 0.0599)	0.9930 (\pm 0.0038)	0.9916 (\pm 0.0046)	0.9929 (\pm 0.0059)	0.9989 (\pm 0.0004)	0.9976 (\pm 0.0016)	0.9988 (\pm 0.0010)	0.9687 (\pm 0.0286)	0.9436 (\pm 0.0203)	0.9723 (\pm 0.0140)
NPE	0.6118 (\pm 0.0155)	0.5830 (\pm 0.0240)	0.5818 (\pm 0.0158)	0.5472 (\pm 0.0076)	0.5238 (\pm 0.0112)	0.5266 (\pm 0.0037)	0.5562 (\pm 0.0147)	0.5292 (\pm 0.0068)	0.5256 (\pm 0.0066)	0.8996 (\pm 0.0206)	0.8502 (\pm 0.0174)	0.8546 (\pm 0.0213)
JANA	0.6146 (\pm 0.0066)	0.5955 (\pm 0.0026)	0.5854 (\pm 0.0037)	0.9905 (\pm 0.0028)	0.9903 (\pm 0.0003)	0.9904 (\pm 0.0009)	0.9845 (\pm 0.0027)	0.9854 (\pm 0.0021)	0.9879 (\pm 0.0011)	0.8707 (\pm 0.0345)	0.8421 (\pm 0.0292)	0.7791 (\pm 0.0232)
APT	0.5457 (\pm 0.0058)	0.5425 (\pm 0.0124)	0.5467 (\pm 0.0050)	0.5367 (\pm 0.0038)	0.5293 (\pm 0.0052)	0.5258 (\pm 0.0047)	0.5401 (\pm 0.0115)	0.5302 (\pm 0.0069)	0.5264 (\pm 0.0075)	0.8164 (\pm 0.0295)	0.6882 (\pm 0.0342)	0.6473 (\pm 0.0343)
CP-VAE	0.7328 (\pm 0.0347)	0.7492 (\pm 0.0496)	0.7482 (\pm 0.0228)	0.6309 (\pm 0.0357)	0.6003 (\pm 0.0165)	0.5851 (\pm 0.0355)	0.7854 (\pm 0.0269)	0.7169 (\pm 0.0332)	0.6886 (\pm 0.0637)	0.9279 (\pm 0.0040)	0.8987 (\pm 0.0164)	0.8582 (\pm 0.0148)
UP-VAE	0.7977 (\pm 0.0390)	0.8134 (\pm 0.0395)	0.8032 (\pm 0.0418)	0.7704 (\pm 0.0461)	0.6037 (\pm 0.0318)	0.7530 (\pm 0.0060)	0.8024 (\pm 0.0156)	0.7898 (\pm 0.0137)	0.7549 (\pm 0.0276)	0.9578 (\pm 0.0168)	0.9417 (\pm 0.0114)	0.9409 (\pm 0.0162)

8.2 MMD

Maximum Mean Discrepancy (MMD) is a statistical test used to compare two probability distributions by measuring the difference between their means in a high-dimensional feature space [?]. In the context of SBI, MMD can be used to measure the similarity between the generated and the reference posteriors. Let P and Q be the two distributions being compared, and let ϕ be a feature mapping function that projects the data into a reproducing kernel Hilbert space (RKHS) \mathcal{H} , then MMD is defined as:

$$\text{MMD}^2(P, Q; \mathcal{H}) = \|\mathbb{E}_{x \sim P}[\phi(x)] - \mathbb{E}_{y \sim Q}[\phi(y)]\|_{\mathcal{H}}^2, \tag{16}$$

where, $\mathbb{E}_{x \sim P}[\phi(x)]$ is the mean embedding of the distribution P , and $\mathbb{E}_{y \sim Q}[\phi(y)]$ is the mean embedding of the distribution Q . The norm $\|\cdot\|_{\mathcal{H}}$ measures the distance between these mean embeddings in the RKHS. The MMD^2 value quantifies the squared distance between the mean embeddings of the two distributions within the

RKHS. A MMD² value close to zero indicates that the distributions P and Q are similar, while a larger value suggests significant differences.

Table 7: MMD metric for different methods across simulation budgets (mean \pm std. dev.).

(a) SLCP Distractors, Bernoulli GLM Raw, Lotka Volterra.

Method	SLCP Distractors			Bernoulli GLM Raw			Lotka Volterra		
	Budget	10,000	20,000	30,000	10,000	20,000	30,000	10,000	20,000
GATSBI	5.1993 (\pm 1.232)	7.2478 (\pm 1.2260)	3.0631 (\pm 0.3244)	3.4369 (\pm 0.8517)	4.3479 (\pm 0.5433)	3.5950 (\pm 0.8613)	7.2684 (\pm 0.5733)	5.5183 (\pm 1.7126)	4.8858 (\pm 1.2146)
NPE	1.2167 (\pm 0.2397)	0.7834 (\pm 0.3453)	0.6428 (\pm 0.1779)	1.1227 (\pm 0.0987)	1.1389 (\pm 0.1878)	1.1448 (\pm 0.1287)	2.6357 (\pm 0.3468)	3.8635 (\pm 0.2770)	4.3310 (\pm 0.0709)
JANA	3.4834 (\pm 1.0817)	3.1234 (\pm 0.1769)	3.0176 (\pm 0.8765)	7.6642 (\pm 1.5789)	10.4712 (\pm 0.9031)	11.3721 (\pm 0.2927)	4.8826 (\pm 0.8294)	3.7653 (\pm 0.4288)	3.8278 (\pm 0.5220)
APT	1.8380 (\pm 0.4448)	0.8278 (\pm 0.2373)	0.4422 (\pm 0.1428)	0.7233 (\pm 0.2131)	0.6968 (\pm 0.0826)	0.5437 (\pm 0.1333)	3.1921 (\pm 0.8198)	3.2722 (\pm 0.8169)	4.4739 (\pm 0.9642)
CP-VAE	3.8511 (\pm 1.4076)	1.8129 (\pm 0.6628)	1.2052 (\pm 0.6557)	2.1708 (\pm 0.0391)	1.6792 (\pm 0.3563)	1.6827 (\pm 0.0000)	3.1960 (\pm 0.3824)	3.2443 (\pm 0.2162)	3.4280 (\pm 0.2793)
UP-VAE	1.97623 (\pm 0.3219)	1.5244 (\pm 0.1978)	1.4353 (\pm 0.1306)	1.2034 (\pm 0.6426)	1.6952 (\pm 1.0074)	1.1553 (\pm 0.8829)	4.4367 (\pm 0.7106)	6.1012 (\pm 0.5511)	6.0285 (\pm 1.1408)

(b) Gaussian Mixture, Gaussian Linear, Gaussian Linear Uniform, SLCP.

Method	Gaussian Mixture			Gaussian Linear			Gaussian Linear Uniform			SLCP		
	Budget	10,000	20,000	30,000	10,000	20,000	30,000	10,000	20,000	30,000	10,000	20,000
GATSBI	0.2242 (\pm 0.0296)	0.1149 (\pm 0.0549)	0.1733 (\pm 0.1082)	0.4999 (\pm 0.1595)	0.6476 (\pm 0.3050)	0.7182 (\pm 0.2839)	0.9044 (\pm 0.2353)	0.7712 (\pm 0.1483)	1.1197 (\pm 0.4795)	0.7197 (\pm 0.5598)	0.3375 (\pm 0.1473)	0.7948 (\pm 0.5992)
NPE	0.0604 (\pm 0.0260)	0.0418 (\pm 0.0211)	0.0554 (\pm 0.0347)	0.0105 (\pm 0.0036)	0.0074 (\pm 0.0018)	0.0082 (\pm 0.0011)	0.0258 (\pm 0.0098)	0.0117 (\pm 0.0041)	0.0121 (\pm 0.0051)	0.4021 (\pm 0.0551)	0.1632 (\pm 0.0684)	0.2333 (\pm 0.0935)
JANA	0.0579 (\pm 0.0079)	0.0415 (\pm 0.0037)	0.0383 (\pm 0.0042)	0.5375 (\pm 0.0367)	0.5245 (\pm 0.0072)	0.5169 (\pm 0.0028)	0.5798 (\pm 0.0357)	0.5875 (\pm 0.0279)	0.6181 (\pm 0.0128)	0.3673 (\pm 0.2011)	0.2045 (\pm 0.0917)	0.1209 (\pm 0.0456)
APT	0.0137 (\pm 0.0031)	0.0108 (\pm 0.0088)	0.0110 (\pm 0.0034)	0.0075 (\pm 0.0013)	0.0070 (\pm 0.0018)	0.0080 (\pm 0.0008)	0.0166 (\pm 0.0087)	0.0138 (\pm 0.0053)	0.0113 (\pm 0.0039)	0.1405 (\pm 0.0347)	0.0487 (\pm 0.0296)	0.0287 (\pm 0.0166)
CP-VAE	0.1846 (\pm 0.0602)	0.2623 (\pm 0.1369)	0.2209 (\pm 0.0587)	0.0382 (\pm 0.0131)	0.0220 (\pm 0.0058)	0.0216 (\pm 0.0081)	0.0829 (\pm 0.0295)	0.0448 (\pm 0.0070)	0.0363 (\pm 0.0130)	0.4309 (\pm 0.1369)	0.2488 (\pm 0.0557)	0.1658 (\pm 0.0881)
UP-VAE	0.3081 (\pm 0.1534)	0.3927 (\pm 0.1208)	0.3684 (\pm 0.0876)	0.0611 (\pm 0.0207)	0.0121 (\pm 0.0036)	0.0446 (\pm 0.0025)	0.0912 (\pm 0.0143)	0.1315 (\pm 0.0293)	0.1246 (\pm 0.0187)	0.4740 (\pm 0.1183)	0.4042 (\pm 0.1181)	0.3946 (\pm 0.1852)

9 Discussion

Based on the results presented in the previous sections, we evaluate different methods across low-dimensional, high-dimensional, complex posterior, noisy, and time-series problems. For low-dimensional problems (e.g., Two Moons, Gaussian Mixture), CP-VAE and UP-VAE, successfully capture the true posterior distributions. For the Two Moons test problem, all models effectively recover the bimodal distribution and the crescent shape, except for GATSBI, which captures the bimodal structure but struggles with the intricate crescent form. In case of the Gaussian Mixture model, all methods accurately identify the shared mean of the two Gaussian distributions. Flow-based approaches perform exceptionally well in these scenarios, followed by the variational methods. As the Gaussian mixture test problem entails dependencies between parameters, JANA is particularly effective by virtue of its autoregressive nature. While GATSBI performs adequately, it misses finer details, such as complex shapes, consistent with findings reported in the original GATSBI paper [Ramesh et al., 2022].

For high-dimensional problems (Gaussian Linear, Gaussian Linear Uniform, Bernoulli GLM), CP-VAE and UP-VAE consistently produce accurate posterior approximations with improved uncertainty estimates. While other methods performed well, GATSBI and JANA, despite identifying the correct regions, struggled to accurately capture the variance. As JANA entails factorization of the posterior as a series of parameter-wise conditionals, distractors hinder JANA to an extent.

In complex and noisy problems (SLCP, SLCP with Distractors, Bernoulli GLM Raw), the variational models demonstrate robustness but face certain challenges. SLCP presents a complex posterior, with varying distributions across dimensions and bimodal behavior in two parameters. Both UP-VAE and CP-VAE capture the overall trends, though UP-VAE struggles particularly with dimensions exhibiting bimodal distributions. SLCP with Distractors is even more challenging, consisting of 92 uninformative and 8 informative dimensions. This

complexity affects the variational methods, as CP-VAE’s prior takes the observed data as input, and noisy data impairs its learning capability. Similarly, the dual decoder structure of UP-VAE, with a reconstruction component for observed data, hampers its performance under noisy conditions. Most methods struggle with SLCP Distractors, except for APT which leverages its sequential design to better estimate the posterior. For the Bernoulli GLM Raw case, UP-VAE outperforms CP-VAE, while both GATSBI and JANA face challenges. GATSBI successfully identifies the correct region but exhibits very small variance, whereas JANA accurately infers four dimensions but struggles with the remaining dimensions.

For time-series problems (Lotka-Volterra, SIR), CP-VAE proved to be a better fit than UP-VAE. The reference posterior for Lotka-Volterra has a very small variance, making accurate inference challenging for all models. JANA manages to capture all parameters accurately but still exhibits larger variance compared to the true distribution. For the SIR model, CP-VAE performs comparably to flow-based methods, while UP-VAE struggles with large variance, likely due to its dual-decoder structure that may overemphasize reconstruction. GATSBI, although able to capture the overall trend, underestimates the variance, indicating a tendency to underestimate uncertainty in tight posterior regions.

Sequential flow-based methods, such as APT perform well overall, but can be time-consuming due to the need for multiple rounds of inference. Flow-based methods were generally more accurate, which is expected as they directly target the exact posterior, whereas variational methods, like CP-VAE and UP-VAE, optimize a lower bound on the posterior, leading to potential underestimation of uncertainty and outliers in some cases. We also observed that VAE-based architectures tend to be more accurate and stable compared to GANs. However, managing multiple loss terms, as in UP-VAE, can be challenging, particularly with noisy data and distractors. Additionally, learning the correct prior distribution, as in CP-VAE, can be difficult because the model relies on observed data to inform the prior. If the data contains significant noise or uninformative features, the learned prior may not accurately represent the true underlying distribution, leading to suboptimal posterior approximations. Despite these challenges, VAE-based architectures still provide fast and reliable inference, particularly for high-dimensional problems.

References

- Martin Arjovsky and Leon Bottou. Towards principled methods for training generative adversarial networks, 2022.
- Martin Arjovsky, Soumith Chintala, and Léon Bottou. Wasserstein generative adversarial networks. In *International conference on machine learning*, pages 214–223. PMLR, 2017.
- Kyle Cranmer, Johann Brehmer, and Gilles Louppe. The frontier of simulation-based inference. *Proceedings of the National Academy of Sciences*, 117(48):30055–30062, 2020.
- Jerome H Friedman. On multivariate goodness-of-fit and two-sample testing. *Statistical Problems in Particle Physics, Astrophysics, and Cosmology*, 1:311, 2003.
- Manuel Glöckler, Michael Deistler, and Jakob H. Macke. Variational methods for simulation-based inference. In *International Conference on Learning Representations*, 2022. URL <https://openreview.net/forum?id=kZOUYdhqkNY>.
- Manuel Gloeckler, Michael Deistler, Christian Dietrich Weilbach, Frank Wood, and Jakob H Macke. All-in-one simulation-based inference. In *Forty-first International Conference on Machine Learning*.
- Pedro J Gonzalves, Jan-Matthis Lueckmann, Michael Deistler, Marcel Nonnenmacher, Kaan Öcal, Giacomo Bassetto, Chaitanya Chintaluri, William F Podlaski, Sara A Haddad, Tim P Vogels, David S Greenberg, and Jakob H Macke. Training deep neural density estimators to identify mechanistic models of neural dynamics. *eLife*, 9:e56261, sep 2020. ISSN 2050-084X. doi: 10.7554/eLife.56261. URL <https://doi.org/10.7554/eLife.56261>.
- David Greenberg, Marcel Nonnenmacher, and Jakob Macke. Automatic posterior transformation for likelihood-free inference. In *International Conference on Machine Learning*, pages 2404–2414. PMLR, 2019.
- Joeri Hermans, Volodimir Begy, and Gilles Louppe. Likelihood-free mcmc with amortized approximate ratio estimators. In *International conference on machine learning*, pages 4239–4248. PMLR, 2020.

- Oleg Ivanov, Michael Figurnov, and Dmitry Vetrov. Variational autoencoder with arbitrary conditioning. In *International Conference on Learning Representations*, 2019. URL <https://openreview.net/forum?id=SyxtJh0qYm>.
- Michael I Jordan, Zoubin Ghahramani, Tommi S Jaakkola, and Lawrence K Saul. An introduction to variational methods for graphical models. *Machine learning*, 37(2):183–233, 1999. doi: 10.1023/A:1007665907178.
- Diederik P. Kingma and Max Welling. Auto-encoding variational bayes. In *2nd International Conference on Learning Representations, ICLR 2014*, 2014. URL <http://arxiv.org/abs/1312.6114v10>.
- Alexander Lavin, Hector Zenil, Brooks Paige, David C. Krakauer, Justin Emile Gottschlich, Timothy G. Mattson, Anima Anandkumar, Sanjay Choudry, Kamil Rocki, Atilim Gunecs Baydin, Carina E. A. Prunkl, Olexandr Isayev, Erik J Peterson, Peter Leonard McMahon, Jakob H. Macke, Kyle Cranmer, Jiaxin Zhang, Haruko Murakami Wainwright, Adi Hanuka, Manuela M. Veloso, Samuel A. Assefa, Stephan Zheng, and Avi Pfeffer. Simulation intelligence: Towards a new generation of scientific methods. *ArXiv*, abs/2112.03235, 2021. URL <https://api.semanticscholar.org/CorpusID:244909059>.
- Jan-Matthis Lueckmann, Pedro J Goncalves, Giacomo Bassetto, Kaan Öcal, Marcel Nonnenmacher, and Jakob H Macke. Flexible statistical inference for mechanistic models of neural dynamics. In *Advances in Neural Information Processing Systems*, volume 30. Curran Associates, Inc., 2017. URL https://proceedings.neurips.cc/paper_files/paper/2017/file/addfa9b7e234254d26e9c7f2af1005cb-Paper.pdf.
- Jan-Matthis Lueckmann, Jan Boelts, David Greenberg, Pedro Goncalves, and Jakob Macke. Benchmarking simulation-based inference. In *Proceedings of The 24th International Conference on Artificial Intelligence and Statistics*, volume 130 of *Proceedings of Machine Learning Research*, pages 343–351. PMLR, 13–15 Apr 2021.
- George Papamakarios and Iain Murray. Fast ϵ -free inference of simulation models with bayesian conditional density estimation. *Advances in neural information processing systems*, 29, 2016.
- Stefan T Radev, Marvin Schmitt, Valentin Pratz, Umberto Picchini, Ullrich Köthe, and Paul-Christian Bürkner. Jana: Jointly amortized neural approximation of complex bayesian models. In *Uncertainty in Artificial Intelligence*, pages 1695–1706. PMLR, 2023a.
- Stefan T. Radev, Marvin Schmitt, Lukas Schumacher, Lasse Elsemüller, Valentin Pratz, Yannik Schälte, Ullrich Köthe, and Paul-Christian Bürkner. BayesFlow: Amortized Bayesian workflows with neural networks. *Journal of Open Source Software*, 8(89):5702, 2023b.
- Poornima Ramesh, Jan-Matthis Lueckmann, Jan Boelts, Álvaro Tejero-Cantero, David S. Greenberg, Pedro J. Goncalves, and Jakob H. Macke. GATSBI: Generative adversarial training for simulation-based inference. In *International Conference on Learning Representations*, 2022. URL <https://openreview.net/forum?id=kR1hC6j48Tp>.
- Danilo Rezende and Shakir Mohamed. Variational inference with normalizing flows. In *International conference on machine learning*, pages 1530–1538. PMLR, 2015.
- Ivaxi Sheth and Samira Ebrahimi Kahou. Auxiliary losses for learning generalizable concept-based models. In *Proceedings of the 37th International Conference on Neural Information Processing Systems*, NeurIPS ’23, Red Hook, NY, USA, 2024. Curran Associates Inc.
- Scott A Sisson, Yanan Fan, and Mark Beaumont. *Handbook of approximate Bayesian computation*. CRC press, 2018.
- Kihyuk Sohn, Honglak Lee, and Xinchen Yan. Learning structured output representation using deep conditional generative models. *Advances in neural information processing systems*, 28, 2015.
- Daniel Ward, Patrick Cannon, Mark Beaumont, Matteo Fasiolo, and Sebastian Schmon. Robust neural posterior estimation and statistical model criticism. *Advances in Neural Information Processing Systems*, 35:33845–33859, 2022.
- Samuel Wiqvist, Jes Frelsen, and Umberto Picchini. Sequential neural posterior and likelihood approximation, 2021.

Andrew Zammit-Mangion, Matthew Sainsbury-Dale, and Raphaël Huser. Neural methods for amortised parameter inference. *arXiv preprint arXiv:2404.12484*, 2024.